Numerical Simulation of an Explosively Deepening Cyclone in the Eastern Pacific

YING-HWA KUO

National Center for Atmospheric Research, Boulder, Colorado*

RICHARD J. REED

Department of Atmospheric Sciences, University of Washington, Seattle, Washington

(Manuscript received 15 December 1987, in final form 26 April 1988)

ABSTRACT

A series of nine experiments were conducted using a version of the Pennsylvania State University/National Center for Atmospheric Research (PSU/NCAR) mesoscale model. Objectives were: 1) to test the ability of a high resolution limited-area model to simulate an extraordinary cyclogenesis that occurred in the eastern Pacific in November 1981; 2) to examine the effects of various physical processes on the storm development and 3) to determine the reasons for the failure of the operational Limited-area Fine-mesh Model (LFM) to forecast the event. Six of the experiments employed a 40 km grid and three employed an 80 km grid. Initial data for seven of the experiments consist of fields interpolated from the National Meteorological Center (NMC) operational analysis supplemented by subjective soundings created by Reed and Albright. The supplementary data were withheld in two of the experiments. Principal findings are:

1) The control experiment, which utilized the supplementary dataset, a 40 km grid and an explicit moisture scheme, simulated a major cyclone with a central pressure of 969 mb and a deepening rate of 31 mb per 24 h (observed values were 950 mb and 48 mb per 24 h). The path of the cyclone was well predicted, as were several features of the storm that could be verified by satellite and aircraft observations.

2) A vertical cross section taken immediately ahead of the storm center at the time of rapid deepening revealed a symmetrically neutral or slightly unstable state in and near the warm frontal zone and a narrow, sloping sheet of rapidly ascending air ($w > 50$ cm s^{-1}) at the frontal boundary. Low-level convergence exceeded 1.0×10^{-4} s^{-1} as the air approached the zone. Vorticity grew from near zero to 6–7 f in only a few hours.

3) Moist processes were essential to the rapid development. Dry simulations produced deepenings of only 13–15 mb in the 24 hour period, implying that roughly half the intensification in the control experiment can be ascribed to dry baroclinicity and half to latent heat release and its interactions with baroclinicity.

4) Surface energy fluxes had no significant impact on the development during the 24 hour period of rapid deepening.

5) An experiment with parameterized convective and nonconvective precipitation yielded essentially the same final pressure as the control experiment. However, the time of most rapid deepening was delayed in the simulation with parameterized convection. The delay was related to differences in the vertical heating profile in the two experiments.

6) Reduction of the grid size from 80 km to 40 km had only a minor effect on the central pressure, suggesting that further reduction would not eliminate the 19 mb error in the predicted central pressure.

7) A considerably weaker cyclone (982 mb vs 971 mb central pressure) resulted when the supplementary data were withheld in an experiment conducted on the 80 km grid.

8) An experiment designed to match most closely the conditions of the LFM forecast yielded the weakest development of all. It is speculated that the absence of development in the LFM forecast stemmed from shortcomings of the initial analysis.

9) A possible cause of the failure of the present experiments to fully capture the storm intensity is the deficiency of middle and upper-level observations, and the attendant uncertainties in the upper-level analyses, in the prestorm period.

1. Introduction

On 13 November 1981 an extreme case of explosive cyclogenesis took place in a section of the Eastern Pacific where such events are climatologically rare (Roebber 1984). During the 24 hour period from 0000 UTC 13 November to 0000 UTC 14 November, the central pressure of the storm fell by approximately 50 mb to an estimated depth of 950 mb. In a single 6 hour period, from 1200 to 1800 UTC 13 November, the storm deepened more than 20 mb. Several ships caught in the storm reported winds of 25 m s^{-1} or greater and two ships recorded speeds in excess of 45 m s^{-1}.

The Limited-area Fine-mesh Model (LFM) 24 hour forecast initialized at 0000 UTC 13 November com-

* The National Center for Atmospheric Research is sponsored by the National Science Foundation.

Corresponding author address: Dr. Ying-Hwa Kuo, NCAR, P.O. Box 3000, Boulder, CO 80307.

pletely failed to predict the explosive development. Only a weak trough was shown in the vicinity of the storm center on the prognostic surface chart for 0000 UTC 14 November, and the predicted pressure at the storm center was in error by 55 mb. Earlier studies (Leary 1971; Sanders and Gyakum 1980) have indicated that it is not uncommon for operational models to fail to predict explosive cyclogenesis. A recent study (Sanders 1987), however, shows a definite improvement in predictive capability for the western Atlantic, though not for the eastern Pacific. Two examples of notable past failures were the *Queen Elizabeth II* (*QE-II*) storm of September 1978 (Gyakum 1983a,b; Anthes et al. 1983; Uccellini 1986) and the Presidents' Day storm of February 1979 (Bosart 1981; Bosart and Lin 1984; Uccellini et al. 1984, 1985). As a forecast failure of equal or even greater magnitude, the November 1981 storm presents an unusual opportunity for further study of the problem of simulating and predicting explosive cyclogenesis.

A synoptic study of the event has already been conducted by Reed and Albright (1986, hereafter referred to as RA). Using surface and upper air analyses and satellite imagery, they found that the explosive development took place within a strong baroclinic zone as a shallow frontal wave traveled from the relatively stable environment of a long-wave ridge to the unstable environment of a long-wave trough. A manifestation of the strong baroclinicity was the existence of winds in excess of 90 m s^{-1} at jet stream level upstream of the low center shortly before the rapid deepening. At the same time the frontal cloud band immediately downstream of the low center exhibited near neutral lapse rates and a symmetrically unstable state. The Reed and Albright study suggests that the explosive development was a consequence of strong, deep baroclinic forcing acting on an environment that was neutral or slightly stable with respect to moist upright convection and unstable with respect to slantwise convection.

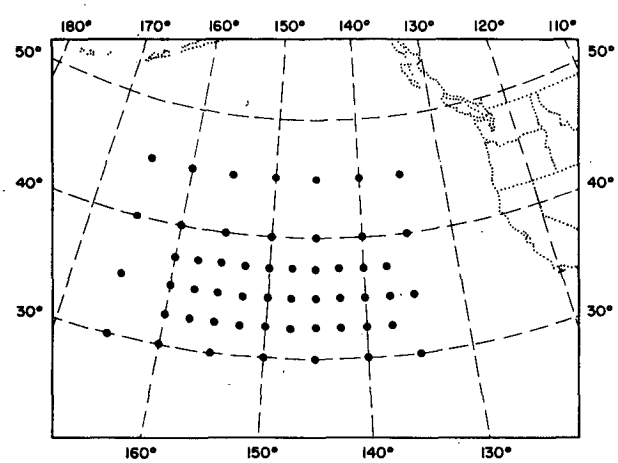

FIG. 1. Domain of model simulation. Locations of supplementary soundings are indicated by solid dots.

In view of the limited observations over the ocean, RA did not attempt to describe the structure of the storm in detail or to assess quantitatively the various forcing mechanisms responsible for the storm development. In this sequel to their study, a numerical simulation is presented of the event using the Pennsylvania State University/National Center for Atmospheric Research (PSU/NCAR) mesoscale model. The objectives of this study are: 1) to test the ability of a high resolution mesoscale model to simulate the explosive development, 2) to examine the structure of the storm using the dynamically consistent four-dimensional dataset provided by the model, 3) to compare, to the extent possible, the predicted structure with observed features, 4) to elucidate by means of a series of sensitivity experiments the roles of various physical processes and of grid resolution and initial conditions in the storm development, and 5) to ascertain the cause of the failure of the NMC operational predictions.

2. Model description and experiment design

a. Model description

The version of the PSU/NCAR mesoscale model used here is that described by Anthes et al. (1987). The vertical coordinate is $\sigma = (p - p_t)/(p_s - p_t)$, where p is pressure, p_s is surface pressure, and p_t is the constant pressure at the top of the model (100 mb). The number of σ levels is 16 (0.0, 0.1, 0.2, 0.3, 0.4, 0.5, 0.6, 0.7, 0.78, 0.84, 0.89, 0.93, 0.96, 0.98, 0.99, 1.0), which gives 15 layers of unequal thickness at which the temperature, moisture and wind variables are defined. The computational domain (Fig. 1) contains an array of 91 × 121 grid points, spaced approximately 40 km apart for the first six of the nine experiments conducted. Experiments 7–9 use an 80 km grid interval with a horizontal mesh of 46 × 61 points. A subarea of the forecast domain will be used in the subsequent discussion of the model results.

The parameterization of the surface and planetary boundary layer (PBL), described by Zhang and Anthes (1982), was originally developed by Blackadar (1979). In this scheme, vertical fluxes of heat, moisture and momentum are calculated explicitly between layers. Under stable conditions, the turbulent fluxes are parameterized by a local Richardson number. Under unstable regimes, vertical fluxes are modeled by mixing convective eddies originating at the surface and environmental air in the PBL. Over the ocean, the sea surface temperature is held constant. The surface roughness, z_0, is a function of frictional velocity u_*, (Delsol et al. 1971)

$$z_0 = 0.032 \frac{u_*^2}{g} + z_{0c} \tag{1}$$

where g is gravity, and z_{0c} is a background value of

0.01 cm. It is important to recognize that in this formulation the surface sensible and latent heat fluxes are functions of the surface wind speed.

Three different precipitation schemes are used in this study. In the first, the cumulus parameterization and treatment of nonconvective precipitation follow methods developed by Kuo (1974) and Anthes (1977). If a stability check indicates the possibility of convection, latent heat is released using the vertically integrated moisture convergence in a column and an assumed vertical distribution of convective heating based on the diagnostic heat and moisture budget study of Kuo and Anthes (1984) for midlatitude convection.

In the second option, prognostic equations are included for water vapor, cloud water and rain water. Evaporation in unsaturated layers is considered. This scheme, called the explicit scheme, follows Hsie et al. (1984) and produces precipitation only when a grid point is saturated. This type of scheme was used successfully by Rosenthal (1978) for hurricane simulation, by Ross and Orlanski (1982) for cold front simulation, and by Wang and Orlanski (1987) for simulation of the Tibetan Plateau vortex. The grid sizes used in these previous studies were 20, 61.5 and 96 km, respectively.

It might be argued that the explicit scheme is not realistic, given that convection cannot be resolved with a 40 km grid. However, the counter argument might be made that if the grid size is small enough, this scheme should be more realistic because it does not require the arbitrary closure assumptions contained in most convective parameterizations. As further justification for use of the explicit scheme, we note that the present study deals with an extratropical cyclone in which most of the precipitation and associated latent heat release occur on the subsynoptic scale or in mesoscale slantwise frontal circulations that can be at least partially resolved with a 40 km grid. In any event, we view the use of this scheme as exploratory and aimed at elucidating possible mesoscale mechanism(s) for explosive deepening of extratropical cyclones rather than at faithfully depicting the role of small-scale convection in the storm development.

In the third option, the latent heat of condensation was set to zero with water vapor treated as a passive variable. Consequently, the latent heat release associated with precipitation had no dynamic feedback to the model atmosphere.

b. Initial conditions

Two different sets of initial conditions were used in this study. The first set involves an interpolation of the National Meteorological Center's (NMC) operational global analysis to the model grid. The interpolated analysis is enhanced by available rawinsonde data at mandatory and significant levels through a Cressman-type scheme based on successive scans (Benjamin and Seaman 1985). Since no rawinsonde observations were taken in the area of primary interest, our final analysis is essentially a reproduction of the NMC global analysis. For convenience, we will call it the NMC analysis. As discussed in RA, there are significant deficiencies in the NMC analysis. For example, the intensity of the storm as portrayed in the height and wind fields is too weak and moisture is deficient at the lower levels.

In the second set of initial conditions, the NMC analyses are supplemented by subjective soundings created at the grid points shown by solid dots in Fig. 1. Key elements in creating the subjective soundings were a manual surface analysis based on archived ship data, including reports received after the operational cutoff times, and an analysis of the moisture field based on empirical relationships applied to satellite cloud information. The reanalysis procedure, described in part by RA, is now summarized in full.

1) Within the domain shown in Fig. 1, the subjective surface pressure analysis was compared with the NMC analysis. The change in mean surface to 400 mb temperature, or 1000–400 mb thickness, needed to bring the NMC pressures into agreement with the manual analysis was then determined (assuming the NMC 400 mb height to be essentially correct).

2) The NMC temperature fields at 850, 700 and 500 mb were reanalyzed so that the weighted-mean of the temperature changes at these levels approximately equaled the needed changes in 1000–400 mb mean temperature. Largest changes were made at the 850 mb level and smallest at 500 mb.

3) Virtual temperature profiles were computed at the grid points, based on the revised temperature fields and on estimated dewpoints. Surface dewpoints were derived from an analysis of ship observations, and dewpoints aloft were calculated from standard NMC procedures used in estimating relative humidities from satellite cloud images. Further minor adjustments were made in temperatures in order to avoid superadiabatic lapse rates and to assure that the 1000–400 mb thicknesses at the grid points were unaffected by the virtual temperature correction.

4) A variety of procedures were used to derive winds at the grid points. Surface wind speeds were determined from direct analysis of ship data; surface wind directions from a graph (Brown 1986) that gives the angle between isobar and wind as a function of air–sea temperature difference. Winds at 925 mb were obtained by adding 1000–925 mb thermal winds to the surface wind field. Winds from 850 mb upward were determined from the gradient wind formula using an iterative method. Trajectory curvatures needed in making the gradient wind computations were estimated from an extension of the formula appearing in Holton (1979, p. 66). Streamline curvatures, storm motion and wind changes in a coordinate system moving with the storm were taken into account.

The subjective soundings were treated in the same manner as conventional soundings and were analyzed

to the model grid using the same procedure as that employed in deriving the first set of initial conditions. For each set of initial conditions, a vertical mode initialization procedure (Errico 1986) was used to balance wind and mass fields and to remove inertia-gravity wave oscillations. In this procedure only the first two vertical modes were modified. The moisture field is not changed by the initialization process.

c. *Experiment design*

The experiment design is summarized in Table 1. Nine experiments, including the control (Expt. 1) were carried out. All forecasts or simulations were initialized at 0000 UTC 13 November and were run for 24 hours. The simulations were based on the enhanced analysis provided by RA, except for experiments 8 and 9. The first six experiments used a 40 km grid, while the last three used an 80 km grid. The lateral boundary conditions were obtained from linear interpolation of the NMC 12 hourly analyses.

The control experiment included surface fluxes, friction and the explicit prediction of water vapor, cloud water and rain water without cumulus parameterization. This experiment produced the most realistic simulation of the storm. Experiment 2 was identical to the control, except that the surface sensible and latent heat fluxes were turned off. This experiment tests the impact of surface energy fluxes on the storm development. Experiment 3 was the same as the control experiment except that a different precipitation scheme was employed. The scheme involved parameterizations of convective and nonconvective precipitation without explicit prediction of cloud water and rain water (described as option 1 in section 2a). A comparison between the control and this experiment reveals the impact of the chosen precipitation parameterization scheme on the storm development.

In the next three experiments, the latent heat release associated with condensation was set to zero. In essence these experiments test the extent that the development can be ascribed to dry baroclinicity. Experiment 4, the full physics dry run, was the same as the control, except that the latent heat release was not included. Experiment 5 was the same as Experiment 4, except that the surface fluxes were removed. In Experiment 6, surface friction and surface energy fluxes were turned off.

The last three experiments utilized an 80 km grid. Experiment 7 used the same physical parameterizations as the control. A comparison between this experiment and the control will reveal the impact of grid resolution on the model simulation. Both experiments 8 and 9 were initialized with the NMC analysis. Experiment 8, like Experiment 7, employed the explicit scheme. A comparison between experiments 7 and 8 will show the impact of the supplementary dataset on the prediction of the storm. Experiment 9 used parameterizations of convective and nonconvective precipitation instead of the explicit scheme. Since this experiment employed the unenhanced NMC analysis and the simple Kuo-type convective parameterization, it resembled most closely the conditions of the NMC operational forecast. Of course, with 15 vertical levels and 80 km, the experiment has higher vertical and horizontal resolution than does the LFM.

3. Results of the control experiment and comparisons with results of a dry simulation

In this section, we compare the predicted path and intensity of the storm in the control simulation with the observed path and intensity and present a selection of horizontal maps and vertical cross sections that depict the structure of the simulated storm. Because of the inadequate data network over the ocean, it is difficult to verify many of the simulated features, but thanks to ship and aircraft observations and satellite imagery, some of the selected charts can be used for verification purposes.

a. *Verification of the control simulation*

Figure 2 compares the predicted path and intensity of the storm during the 24 hour simulation period with the observed path and intensity, which is taken from Fig. 12 of RA. It is evident that the predicted track was somewhat to the right of (south and east of) the ob-

TABLE 1. Description of numerical experiments.

Expt.	Surface fluxes	Surface friction	Initial field	Grid size (km)	Moisture cycle
1	yes	yes	NMC + suppl. data	40	explicit scheme
2	no	yes	NMC + suppl. data	40	explicit scheme
3	yes	yes	NMC + suppl. data	40	cumulus para.
4	yes	yes	NMC + suppl. data	40	passive moisture (dry)
5	no	yes	NMC + suppl. data	40	passive moisture (dry)
6	no	no	NMC + suppl. data	40	passive moisture (dry)
7	yes	yes	NMC + suppl. data	80	explicit scheme
8	yes	yes	NMC analysis only	80	explicit scheme
9	yes	yes	NMC analysis only	80	cumulus para.

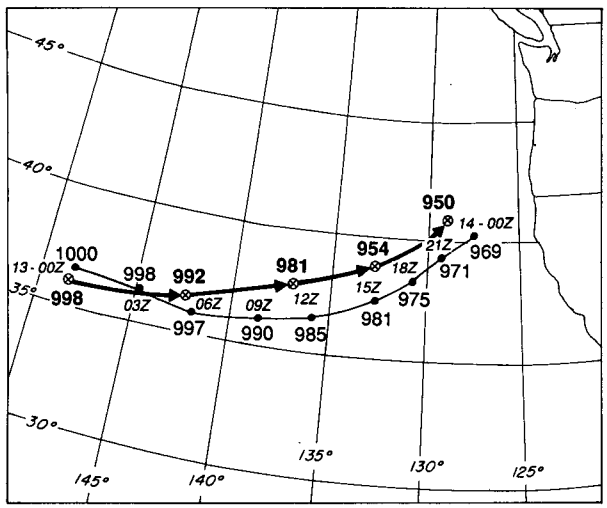

FIG. 2. Comparison of observed path (circles with crosses) and central pressure of the low with the predicted path (solid dots) and central pressure. Positions are every 3 hours for the predicted storm and every 6 hours for the observed.

served track, but the discrepancy is small. Note that the final position of the storm was in error by only 150 km despite a distance of travel of more than 1800 km. The prediction of intensity was less successful. The predicted central pressure after 24 hours was 969 mb; the observed central pressure was estimated to be 950 mb. Although the predicted depth fell short of the observed, the model simulation did succeed in producing a major cyclone and a deepening rate (31 mb per 24 hours) that satisfies the criterion for explosive cyclogenesis (Sanders and Gyakum 1980).

The 12 hour and 24 hour predictions of surface pressure (with superimposed 1000–500 mb thickness) along with the verifying analyses, taken from Fig. 5 of RA, are shown in Figs. 3 and 4. In view of the uncertainty of the analysis at 1200 UTC 13 November (Fig. 3b), arising from the characteristic dearth of ship observations in the Pacific at 1200 UTC, the 12 hour prediction can be described as quite successful. However, from GOES-W imagery (Fig. 6b of RA and Fig. 7b of this article) it seems almost certain that the more southerly path and faster movement of the simulated low represent minor prediction errors.

The 24 hour prediction is less successful (Fig. 4), especially as regards the shape and intensity of the storm. The verifying analysis, based on ample surface data (see Fig. 11b of RA), reveals the existence of a 950 mb center and tightly packed, nearly circular isobars within the core of the storm. The simulated storm is not as deep (969 mb) and is more oval-shaped with a pronounced elongation toward the northeast. Clearly, the simulation failed to reproduce the extreme vortex development described in RA. No further growth in the position error occurred between 1200 UTC 13 November and 0000 UTC 14 November, so the position at the latter time can be regarded as highly satisfactory for a 24 hour forecast of a fast-moving storm.

A feature of the analysis in Fig. 4b, that also appeared in Gyakum's (1983a) analysis of the *QE-II* storm, is the circular region of high thickness in the inner core of the storm. There has been some debate whether such a feature is a real characteristic of intense maritime lows or whether it arises from the uncertainty of the upper-level analyses over the ocean. In the present simulation (Fig. 4a), the warm core is lacking despite the indication of an abnormally low 1000 mb height at the center of the low. An examination of the 500 mb simulation (Fig. 5a) shows the presence of a mesoscale low center aloft displaced only slightly to the west of the surface low. Thus, the 500 mb heights are lower in the vicinity of the surface low than might be

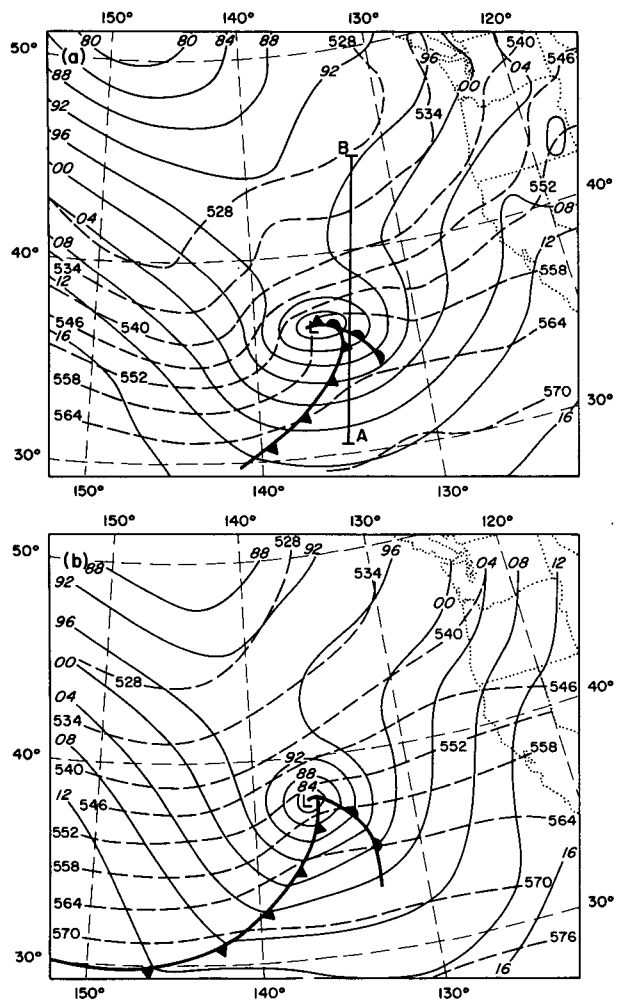

FIG. 3. Sea level pressure at 4 mb intervals (solid) and 1000–500 mb thickness at 60 m intervals (dashed) for (a) 12 hour forecast for control experiment verifying at 1200 UTC 13 November with fronts subjectively added, and (b) the subjective analysis at the same time reproduced from Reed and Albright (1986). Line of later cross sections indicated by AB.

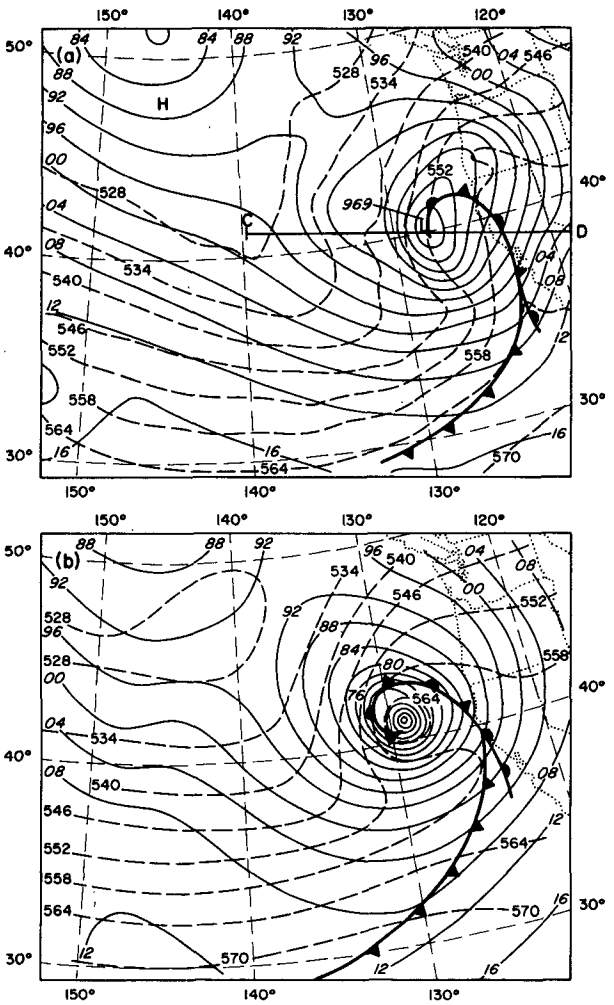

FIG. 4. Sea level pressure (solid) and 1000–500 mb thickness (dashed) for (a) 24 hour forecast for control experiment verifying at 0000 UTC 14 November with fronts subjectively added, and (b) the subjective analysis at the same time reproduced from Reed and Albright (1986). Line of later cross sections indicated by CD.

anticipated, and the thickness is correspondingly less. The NMC final analysis for the same hour (Fig. 5b), based on essentially no middle level data, gives little evidence of the mesoscale feature. If the 1000 mb height pattern of the simulated low were subtracted from the NMC analysis, an artificial warm core would indeed appear in the thickness pattern of the simulation.

Because of the lack of middle level data, it is of interest to inquire whether there is evidence for the mesoscale feature at higher levels where jet aircraft data are available for verifying the prediction. The 300 mb wind forecast for the control simulation (Fig. 6a) does indeed indicate the presence of a sharp trough in the region near and above the surface low that can be regarded as an upward extension of the 500 mb mesolow. Moreover, the existence of this feature in the wind field is substantiated in part by aircraft observations taken within one hour of the standard observation time. Three of the pertinent winds and their respective nearest standard pressure levels are plotted in Fig. 6a. These winds are in remarkable agreement with the simulated flow field, whereas they differ considerably from the NMC analyzed flow field at 300 mb (Fig. 6b). The inset to Fig. 6b shows a series of three aircraft winds measured in the vicinity of the surface low center between 2107 UTC 13 November and 0427 UTC 14 November. Observation times are indicated next to the corresponding positions of the surface center (solid circle). Positions of the center are interpolated from Fig. 12 of RA. Nearest standard pressure levels (mb) are plotted to the left of the winds and thin lines connect the observations with the appropriate times. The development by 0427 UTC of a closed low at 300 mb centered only a short distance to the west of the surface low is strongly suggested.

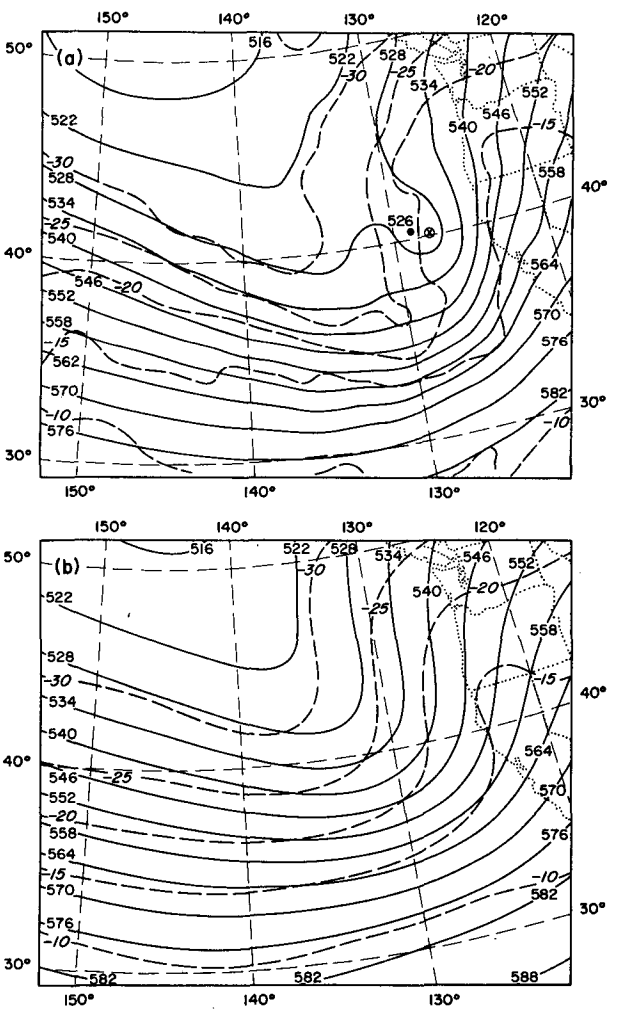

FIG. 5. The 500 mb height (dm, solid) and temperature (°C, dashed) for (a) 24 hour forecast for control experiment verifying at 0000 UTC 14 November, and (b) the NMC analysis at the same time.

The reason why the NMC analysis did not conform more closely to aircraft winds is not known, but the fact that the 24 hour prediction of the PSU/NCAR model was more correct over the ocean than the NMC analysis at the level in question seems incontestable. However, the NMC analysis is more accurate near the coast where a 60 m s^{-1} wind maximum in the model simulation is not supported by nearby land observations. It will be seen later that the successful prediction of the upper-level flow over the ocean hinged critically on latent heat release. On the basis of the foregoing evidence we conclude that it is unwise to assume that intense extratropical oceanic cyclones possess hurricanelike warm cores. In the present case, at least, there is strong evidence that a more accurate upper-level analysis would have eliminated, or much reduced, the warm core seen in Fig. 4b. Admittedly, our conclusion is based on the simulated storm, not on the actual storm. The latter, it will be recalled, possessed a much lower central pressure and therefore an added tendency for a warm core.

Relative humidity forecasts at 400 mb for hour 15 (1500 UTC 13 November) and hour 24 (0000 UTC 14 November) are displayed in Figs. 7a and 8a. A GOES-W water vapor channel image for 1215 UTC and visible image for 2215 UTC 13 November are shown in Figs. 7b and 8b, respectively. Regions with relative humidity of less than 80 percent are shaded in the moisture fields so that the white areas on the maps should correspond to areas of large middle and upper level relative humidity and/or middle and high clouds in the satellite imagery. If allowance is made for the small time differences between forecast fields and satellite pictures, the following features can be said to be in good correspondence: 1) the dark region of low humidity south of the storm center in the satellite picture (Fig. 7b) and the small region of minimum relative humidity (<10 percent) in Fig. 7a; 2) the dark corridor in Fig. 7b and strip of low humidity in Fig. 7a, extending west-northwestward from the aforementioned regions; 3) the region of strong humidity gradient in Fig. 7a and the cloud edge in Fig. 7b (Fig. 6b of RA indicates that the water vapor channel is sensing cloud, not water vapor in the region in question) and 4) the broad swath of high humidity (Fig. 7a) intruding between 30° and 40°N from an upstream storm system and the associated swath of high humidity and/or upper level cloud in Fig. 7b. The only notable shortcoming of the humidity forecast for hour 15 is the lack of a sufficiently broad region of saturation to the southeast of the low center where it appears from the satellite observations that middle and high clouds were almost certainly present.

At 0000 UTC 14 November (Fig. 8a) the aforementioned dry corridor at 400 mb can be seen spiraling into the low center from the west. Also evident in Fig. 8a is the region of strong humidity contrast curling into the storm center from the north and west. The moist swath from the upstream low has merged with the region of saturation in the main storm. The foregoing features are in close agreement with the moisture pattern suggested by the visible image from GOES-W (Fig. 8b).

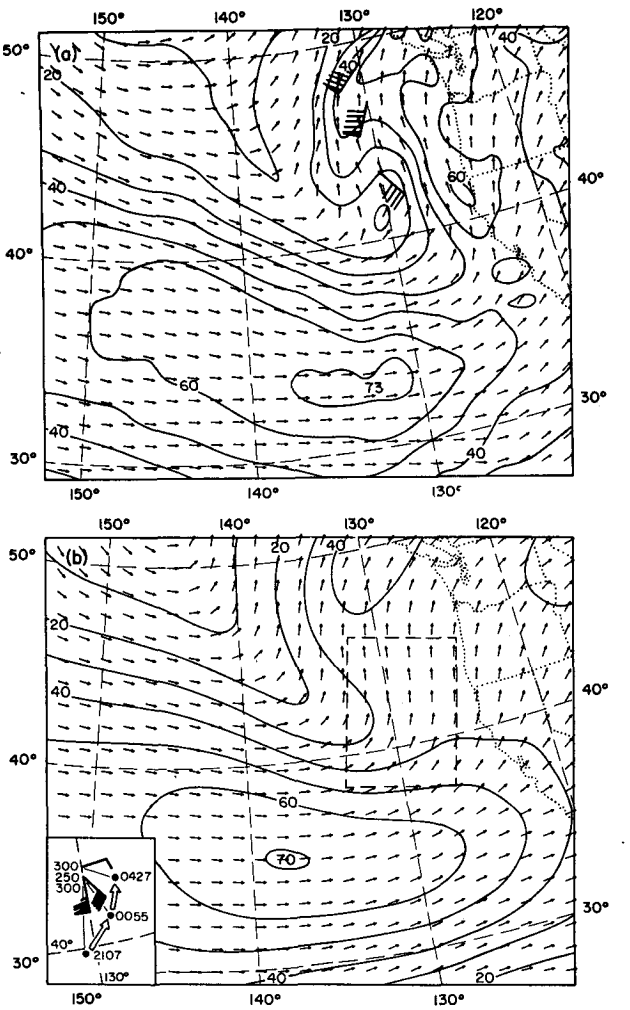

FIG. 6. The 300 mb wind field for (a) 24 hour forecast for control experiment verifying at 0000 UTC 14 November, and (b) the NMC analysis at the same time. Isotachs in m s^{-1}. Wind plots show aircraft measurements taken within one hour of 0000 UTC 14 November. Pennant, 25 m s^{-1}; full barb 5 m s^{-1}. See text for explanation of inset to Fig. 6b. Location of the inset is indicated by the dashed rectangle.

b. *The vertical structure of the simulated storm*

The cross sections in Figs. 9 and 10 illustrate various features of the vertical structure of the storm at 1200 UTC 13 November and 0000 UTC 14 November. The sections for the former time are taken along the line AB in Fig. 3a, those for the latter time along the line CD in Fig. 4a. Shown first (Fig. 9a) are the fields of potential temperature θ (dashed lines) and relative humidity (solid lines). A well-marked frontal zone with a sharp southern boundary (heavy solid line) appears

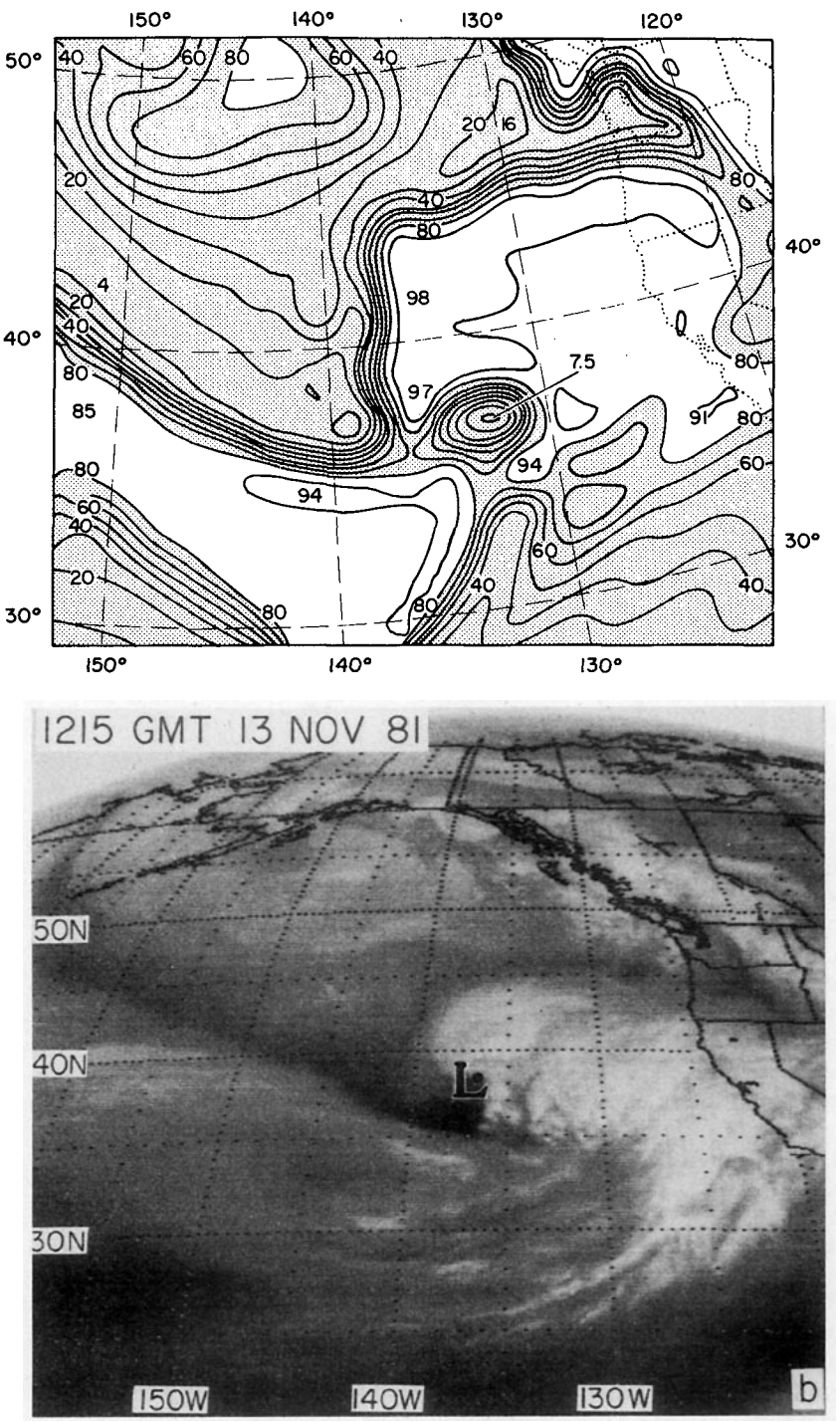

FIG. 7. (a) The 400 mb relative humidity for 15 hour forecast for the control experiment verifying at 1500 UTC 13 November. Areas with RH less than 80 percent are shaded. (b) GOES-W water-vapor channel image for 1215 UTC 13 November 1981. Large dot indicates position of low center.

in the potential temperature field. Humidities indicate saturation in and above the frontal zone. A sliver of dry air appears between 700 and 400 mb immediately to the south of the frontal zone, while a second moist region is observed still farther south. Inspection of horizontal wind and temperature analyses at several levels

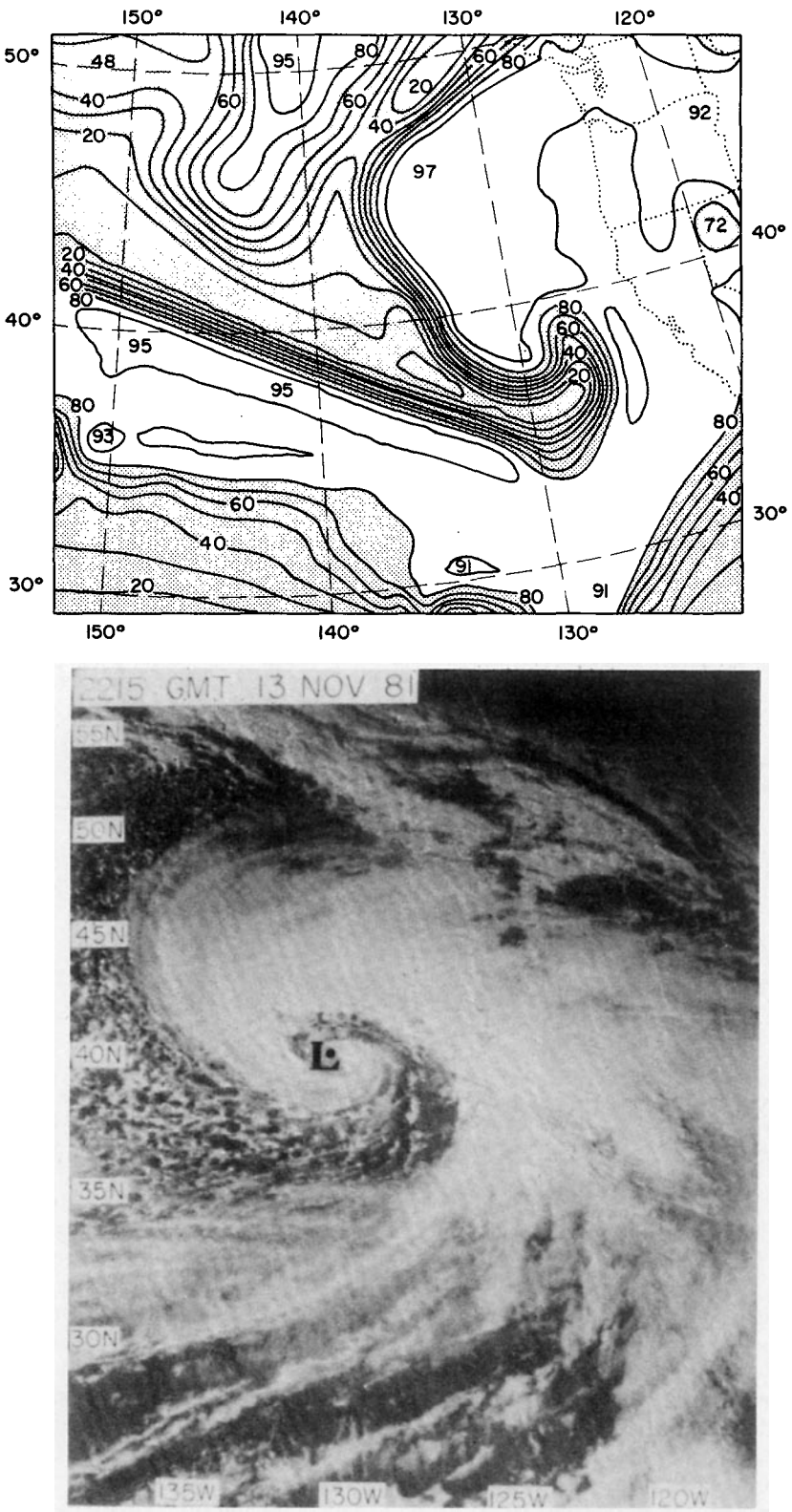

FIG. 8. (a) The 400 mb relative humidity for 24 hour forecast for the control experiment at 24 hour forecast verifying at 0000 UTC 14 November. Areas with RH less than 80 percent are shaded. (b) GOES-W visible images for 2215 UTC 13 November 1981.

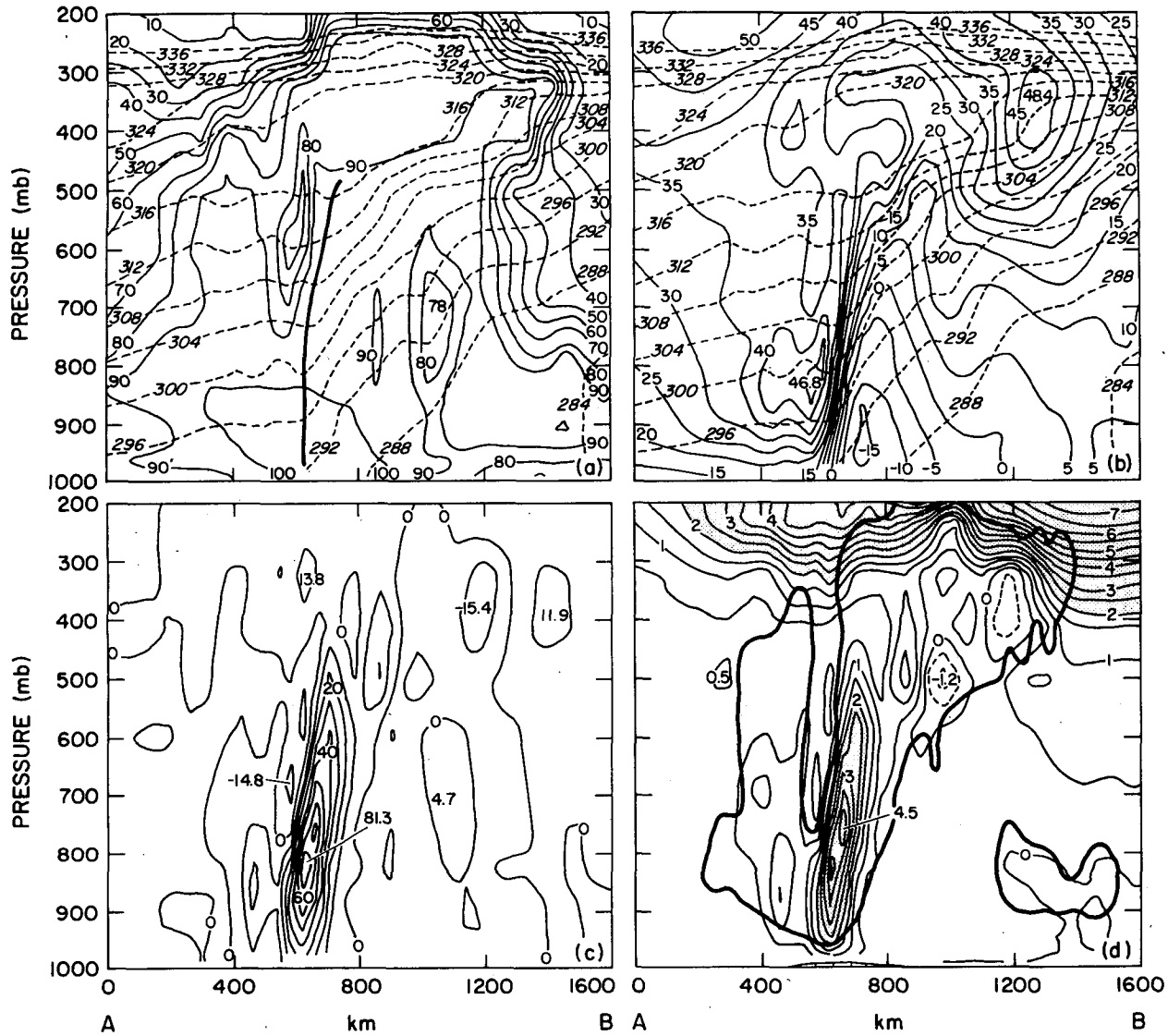

FIG. 9. Vertical cross sections at 1200 UTC 13 November 1981 of (a) relative humidity (solid) and potential temperature (dashed), (b) u component (wind speed perpendicular to the cross section, in m s^{-1}, solid) and potential temperature (dashed), (c) relative vorticity (10^{-5} s^{-1}), and (d) potential vorticity (10^{-7} K kg^{-1} m s). Heavy lines in (a) mark the frontal boundary. Heavy lines in (d) show the outline of cloud boundary. The position of the cross section is indicated on Fig. 3a.

reveals that the dry region lies behind the cold front. At the surface, the cold front is located just to the west of the cross section (Fig. 3a), but in the vicinity of the low center it slopes forward with height and enters the plane of the section. We have not attempted to depict the cold front boundary on the section.

The field of normal wind components (Fig. 9b) features a tight packing of the isotachs in the vicinity of the frontal boundary, especially at lower levels where the velocity changes from nearly 50 m s^{-1} westerly on the warm side of the boundary to more than 15 m s^{-1} easterly on the cool side. A region of weak westerlies appears above the easterlies, dividing the westerly jet stream at 300 mb into two sections. The double jet was not present in the early stages of the forecast, and did not appear at any time in the dry simulations (not shown). The intervening region of light winds in the control simulation formed in proximity to the warm frontal cloud mass. Visual comparison of vertical wind shears and horizontal temperature gradients indicates that the thermal wind relationship is not strongly obeyed. This suggests that accelerations of considerable magnitude were present during the period of rapid development.

Figures 9c and 9d show the vorticity and potential vorticity (PV), respectively, with the area of cloud water depicted on the latter diagram. The potential vorticity is here defined as

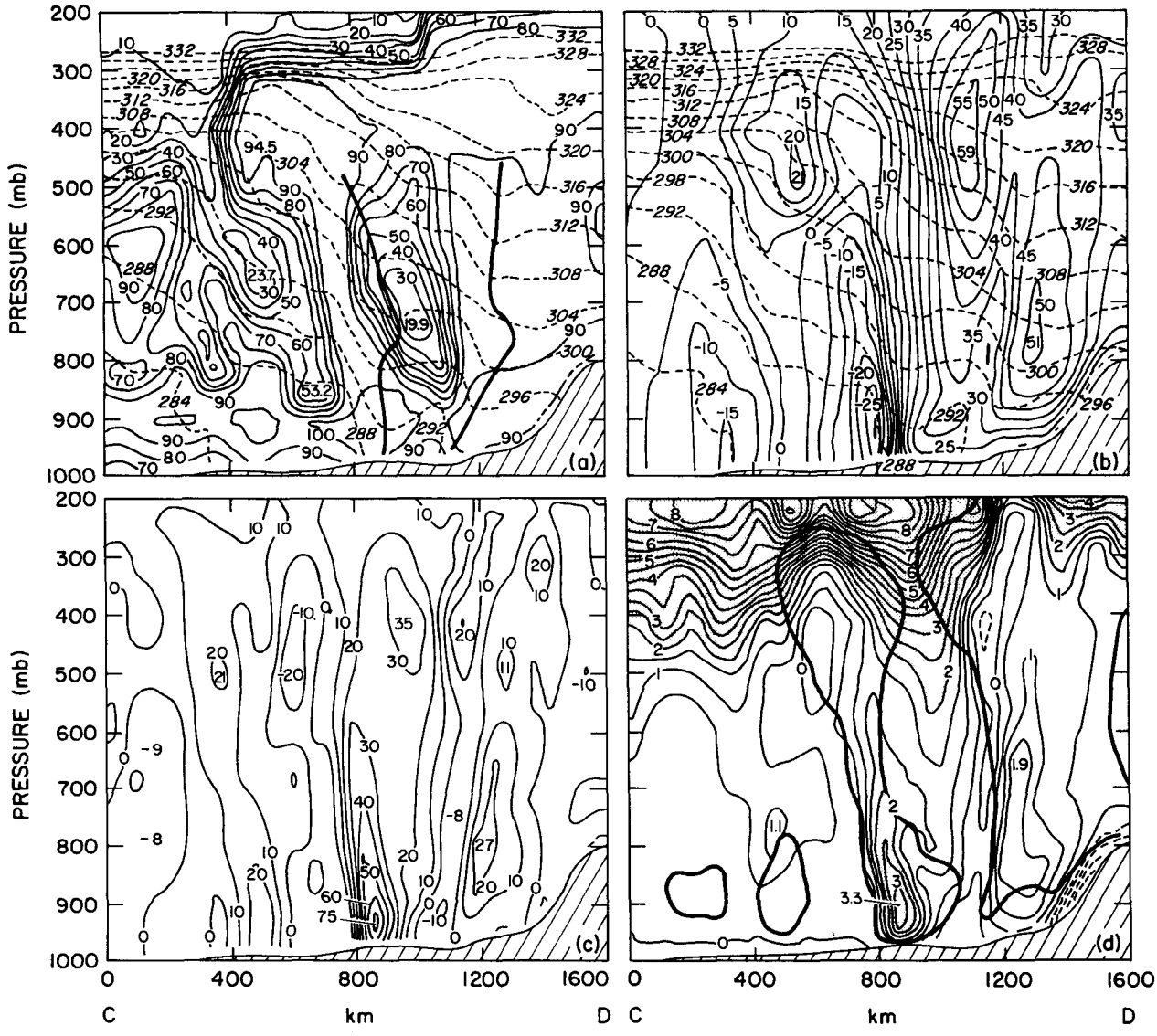

FIG. 10. Vertical cross sections at 0000 UTC 14 November 1981 of (a) relative humidity (solid) and potential temperature (dashed), (b) v component (wind speed perpendicular to the cross section, in m s^{-1}, solid) and potential temperature (dashed), (c) relative vorticity (10^{-5} s^{-1}), and (d) potential vorticity (10^{-7} K kg^{-1} m s). Heavy lines in (a) mark the frontal boundary. Heavy lines in (d) show the outline of cloud boundary. The position of the cross section is indicated on Fig. 4a.

$$\mathrm{PV} = -(\zeta_\theta + f)\frac{\partial \theta}{\partial p}, \qquad (2)$$

where f is Coriolis parameter and $\zeta_\theta = \partial v/\partial x - \partial u/\partial y$ is the vorticity measured on an isentropic surface. From Fig. 9c it is apparent that extremely large vorticity (maximum of 81.3×10^{-5} s^{-1}) exists at lower levels within the frontal zone. The vorticity decreases rapidly with height in the middle troposphere. The potential vorticity (Fig. 9d) shows characteristically large values in the stratosphere. A separate region of large PV with values matching the stratospheric values is located within the frontal cloud band. (For PV defined as above, a value of 2×10^{-7} K kg^{-1} m s is commonly chosen as the lower limit for stratospheric air). In view of the saturation, it is obvious that the large PV in the frontal zone is not the result of advection of stratospheric air but rather is the result of PV production in tropospheric air by latent heat release, as found by Gyakum (1983b) in his study of the *QE-II* storm and by Boyle and Bosart (1986) in their study of a major cyclone development in the Eastern United States. However, examination of horizontal maps of PV (not shown) reveals that values in excess of the above threshold occurred at 500 mb, but not at 700 mb, in dry subsiding air well upstream of the center. This air

was presumably of stratospheric origin. Using the same threshold, Boyle and Bosart (1986) observed true stratospheric air at levels as low as 600 mb upstream of the surface low. In the case of the Presidents' Day storm, Uccellini et al. (1985) identified marginally stratospheric air of high potential vorticity (threshold value of $>1 \times 10^{-7}$ K kg^{-1} m s) at low levels in the region immediately upstream of the cyclone center at a similar stage in the development. Downward penetration of marginally stratospheric air to 800–700 mb was found by Uccellini (1986) in the *QE-II* storm.

A set of cross sections for 0000 UTC 14 November along CD appears in Figs. 10a–d. The potential temperature cross section (Fig. 10a) exhibits two prominent thermal boundaries, marked by the heavy solid lines. Upper level charts (not shown) indicate that the eastern line represents the forward edge of the region of cold advection. Because a classical occlusion process in which the cold front overtakes a preexisting warm front did not occur, the boundary is perhaps best regarded as a forward-sloping cold front. The points separating the cold and occluded fronts in Figs. 4a and 4b are admittedly arbitrarily placed. From a conventional viewpoint, the second boundary can be regarded as the extension of the same front around and to the rear of the low center (Fig. 4a). However, the region of pronounced thermal gradient that exists to its west is not well related to the front but instead seems connected to the region of the enhanced thickness gradient seen in Fig. 4a well to the north of the front.

Troughs of warm air are centered on both thermal boundaries. Examination of the horizontal charts reveals that the troughs are manifestations of a tongue of warm air that extends northward from the warm air source at lower latitudes. From the humidity analysis (Fig. 10a) it is evident that the first trough contains moist, cloudy air and that the second trough lies partly in the cloudy air that encircles the storm from the east and north and partly in the dry air that encircles the storm from the south and west. The cross section provides additional evidence that the simulated cyclone does not possess a warm, dry core similar to that of a hurricane.

The normal wind component (Fig. 10b), as before, exhibits a rapid change at lower levels in the vicinity of the low center. In this section the change is from southerlies to the east of the storm to northerlies to the west. An additional southerly maximum is apparent near 500 mb to the west of the center, separated from the main southerlies by an intervening region of weak southerlies or light northerlies. These features are associated with the mesolow pointed out in the discussion of Fig. 5a.

The vorticity (Fig. 10c) at 0000 UTC 14 November is as strong as earlier (maximum 75×10^{-5} s^{-1}), and the maximum is located even closer to the surface. A secondary maximum appears farther to the east at 400 mb. The extreme value of the near surface vorticity is not implausible. Reed and Albright (1986) commented on a wind report of 28 m s^{-1} from a ship located about 50 km from the low center. A circularly-symmetric cyclone, which is admittedly not an exact representation of the situation, would imply a vorticity near the center of 112×10^{-5} s^{-1}.

The potential vorticity (Fig. 10d) shows a maximum above the low center at 850 mb with values in excess of 2×10^{-7} K kg^{-1} m s extending to about 500 mb. This region again lies within the cloud area and hence must have its origin in tropospheric latent heat release. Downward extensions from the stratosphere of large potential vorticities can be seen just to the east of the low center and considerably to the west. These extensions are associated with low humidities that are indicative of air with stratospheric origin. An examination of horizontal maps of PV (not shown) reveals that air with stratospheric values descended only to 500 mb, or slightly below, and that the stratospheric air formed an arc about the low center. The stratospheric air was not collocated with the vortex, as was inferred to be the case for the Presidents' Day storm (Uccellini et al. 1985).

c. *The role of symmetric instability*

Reed and Albright (1986) presented a meridional cross section (their Fig. 13b) that suggested the presence of a statically neutral and symmetrically unstable state within the frontal cloud band at 0000 UTC 13 November, the starting time of the forecast. Their cross section, constructed from the subjective soundings, intersected the warm front immediately ahead of the low center. The neutral or unstable region, which examination shows was preserved in the model initialization, extended from cloud base to the 500–400 mb levels. On physical grounds a question might be raised regarding the existence of a deep symmetrically unstable layer, since the instability, if present, would be quickly neutralized by slantwise convection (Bennetts and Hoskins 1979; Emanuel 1983) and therefore would not likely be observed. However, one can imagine that *conditional* symmetric instability (Emanuel 1983) existed through a deep layer prior to and during the early stages of cyclogenesis so that it is not unrealistic to pursue the question of how the portrayed symmetric instability affected the evolution of the simulated storm, even if the instability was excessive in the initial analysis. In particular, it is of interest to examine stability conditions for both upright and slantwise convection in the region near the storm center midway through the period of rapid deepening. For this purpose, an additional cross section (Fig. 11) has been prepared along the line AB in Fig. 3a, showing fields of equivalent potential temperature θ_e and absolute momentum M at 1200 UTC 13 November. The absolute momentum, following Eliassen (1962), is defined as $fy - u$, where f is the Coriolis parameter, y the distance along AB (approx-

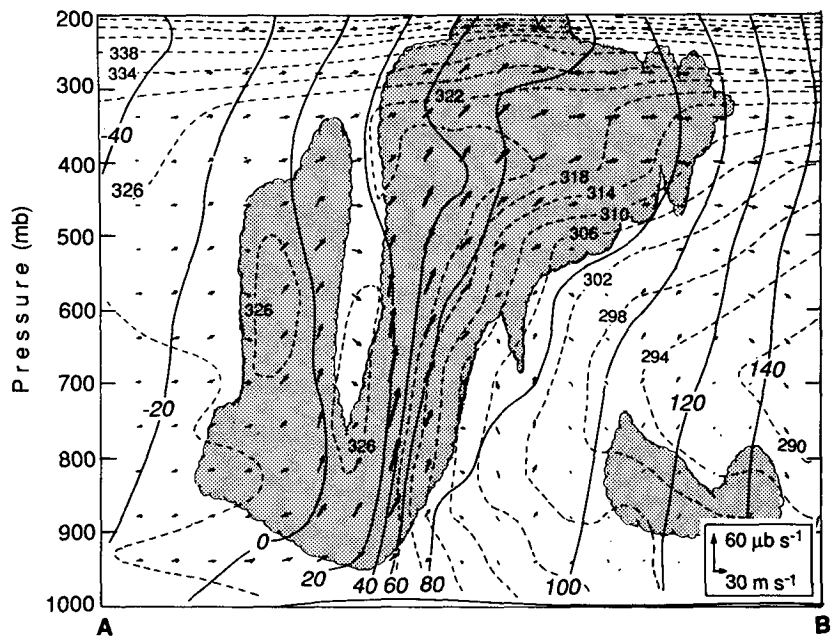

FIG. 11. Cross section along the line AB in Fig. 3a of absolute momentum (solid, m s^{-1}) and equivalent potential temperature (dashed) at 1200 UTC 13 November. Arrows give vertical and horizontal motion in the plane of the cross section according to the attached scale. Shading denotes cloud mass.

imately northward) and u the wind component normal to the section, positive eastward. Stippling on the diagram denotes the region of cloud, as determined from the field of cloud water mixing ratio, and the vectors depict the total two-dimensional flow in the plane of the section. The scale of the horizontal and vertical motions appears in the lower right hand corner of the diagram.

The cross section shows that the air is weakly statically stable and symmetrically neutral (θ_e-lines paralleling M-lines), or in places even slightly symmetrically unstable (θ_e-lines more vertically inclined than the M-lines) in the lower and middle portions of the frontal cloud band. Near the frontal boundary (see Fig. 9a), both within the frontal zone and the immediately adjacent warm air, the velocity vectors indicate the existence of a narrow sloping sheet of rapidly ascending air. Maximum upward motions are approximately 75 cm s^{-1} (70 μb s^{-1}) within the region of upglide. The picture is reminiscent of that presented by Thorpe and Emanuel (1985) in their study of frontogenesis in the presence of small stability to slantwise convection, except that the upward motions are distinctly larger in the present case where neutral or slightly unstable conditions prevail. A two-dimensional model of baroclinic instability in the presence of small stability to moist slantwise convection by Emanuel et al. (1987) also shows the narrow region of enhanced ascent.

Upward motion of the observed magnitude occurring close to the surface produces strong vertical stretching of the boundary layer and associated strong spinup of low-level vorticity. It is apparent that, in the simulation at least, it is the strong sheetlike ascent, made possible by the neutral symmetric stability or slight symmetric instability, that is responsible for the rapid intensification of the vortex and the creation of the extremely large vorticities seen in the cross section presented earlier (Fig. 9c).

The rapidity with which the vorticity spins up is illustrated in Table 2, which gives hourly values of relative vorticity and divergence for air trajectories that at 1500 UTC 13 November were located at the 925 mb level and at the geographical positions A_0, B_0 and C_0 in Fig. 12. Pressures at the beginning and end points of the trajectories are appropriately labeled. The chosen

TABLE 2. Divergences and vorticities (10^{-4} s^{-1}) along selected trajectories.

	A_0		B_0		C_0	
Hour	Div	Vor	Div	Vor	Div	Vor
06	0.08	−0.19	0.13	−0.10	0.50	0.00
07	0.06	−0.20	0.11	−0.09	0.10	−0.03
08	−0.01	−0.20	−0.01	−0.09	0.60	−0.04
09	−0.08	−0.12	−0.07	−0.03	0.70	−0.08
10	−0.09	−0.05	−0.37	0.07	−0.70	−0.08
11	−0.32	0.00	−1.00	0.29	−0.35	0.07
12	−0.66	0.25	−0.70	0.59	−0.13	0.07
13	−1.70	1.70	−1.70	2.70	−1.00	0.30
14	−2.50	5.20	−3.40	4.90	−3.10	2.10
15	−0.59	7.60	−3.80	7.40	−2.70	6.30

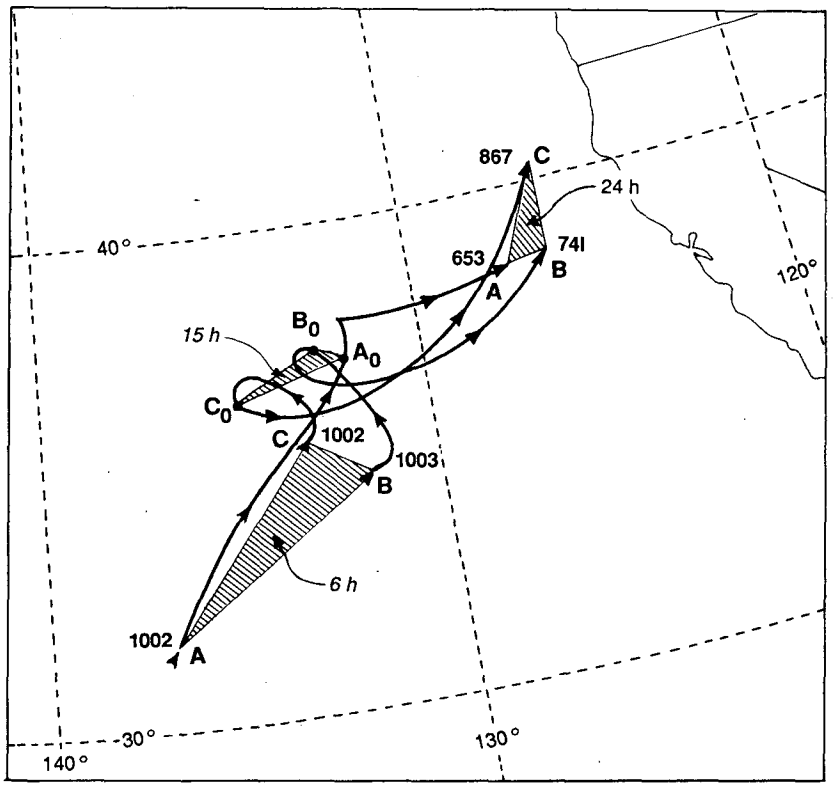

FIG. 12. Trajectories beginning at 0600 UTC 13 November and ending at 0000 UTC 14 November for air parcels that at 1500 UTC 13 November were located at points, A_0, B_0, C_0 and 925 mb. Triangles enclosed by the points are hatched.

points, which bracket the low center, had all acquired relative vorticities in excess of six times the Coriolis parameter at 1500 UTC. From the table it is apparent that the large vorticities were acquired in a brief time span, much of the increase occurring in 3–4 hours. Not surprisingly, the convergences were also extremely large, attaining values in excess of 1×10^{-4} s^{-1} during the period of rapid spinup.

d. Comparisons with the results of a dry simulation

To reveal the impact of latent heat release on the cyclone development we now present results from a dry simulation (Expt. 4) for comparison with those from the control experiment. Shown first (Fig. 13) are the surface pressure and 1000–500 mb thickness simulations for the 12 and 24 hour forecasts, which may be compared with Figs. 3a and 4a. It is evident that the dry storm is considerably weaker than the wet storm and that it moves slower. Noteworthy differences in the thickness pattern also exist. At 1200 UTC 13 November the wet storm exhibits a much stronger thermal gradient to the north and northeast of the low center. Similarly, at 0000 UTC 14 November the wet case possesses a belt of stronger temperature gradient from the Oregon–Washington coast to the region just west and south of the storm center. Some evidence of this feature can be seen in the surface thermal pattern presented in Fig. 11b of RA.

Next, we consider the 24 hour predictions of the 500 mb contour pattern (Fig. 14) and 300 mb flow field (Fig. 15) for the dry simulation. It is apparent from comparison of Fig. 14 with Fig. 5a that the mesolow in Fig. 5a is a product of the moist physics. No evidence of it can be seen in the dry simulation. At the 300 mb level the wind minimum near the surface low center in the wet simulation and the ridge of enhanced wind speeds to the north of the minimum (see Fig. 6a) are likewise products of the latent heat release. Similar features do not appear in Fig. 15, which resembles more closely the NMC 300 mb analysis for 0000 UTC 14 November. (We have already demonstrated that the 24 hour control simulation is in much better agreement with the aircraft winds than the NMC analysis.)

The greater intensity of the wet storm than the dry storm is also reflected in the vertical motion and vorticity fields, as shown by the 12 h forecasts of these fields (Figs. 16 and 17). The maximum upward motion at 700 mb near the low center in the dry run for hour 12 (Fig. 16a) is about 6 μb s^{-1}. In the wet run (Fig. 16b) it is nearly 47 μb s^{-1}. It is evident that the moist processes greatly enhance and concentrate the low-level vorticity, as can be seen by comparing Figs. 17a and

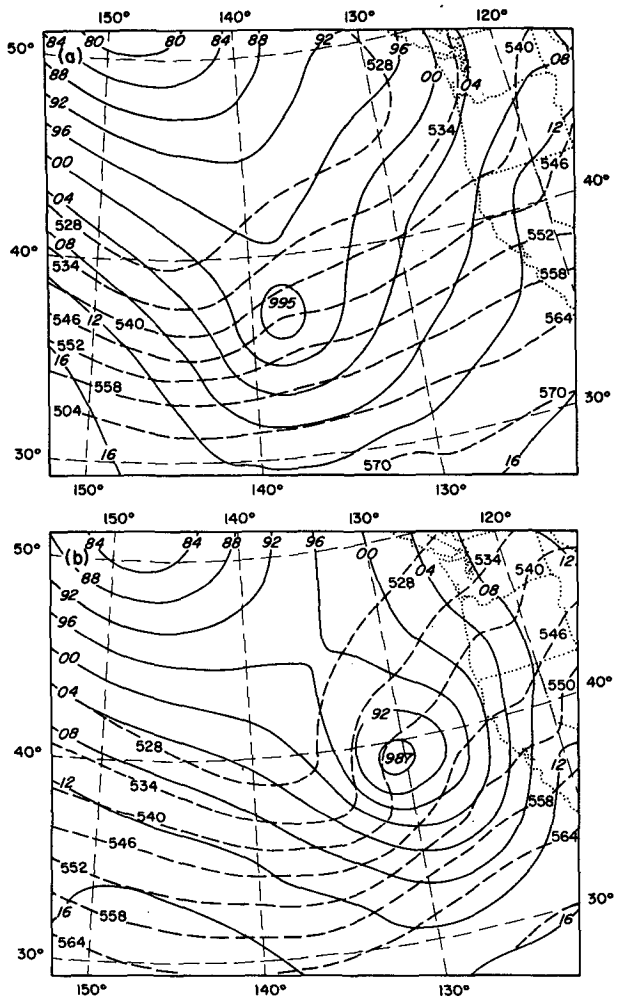

FIG. 13. Sea level pressure (solid) and 1000–500 mb thickness (dashed) for Experiment 4. (a) 12 hour forecast verifying at 1200 UTC 13 November, and (b) 24 hour forecast verifying at 0000 UTC 14 November.

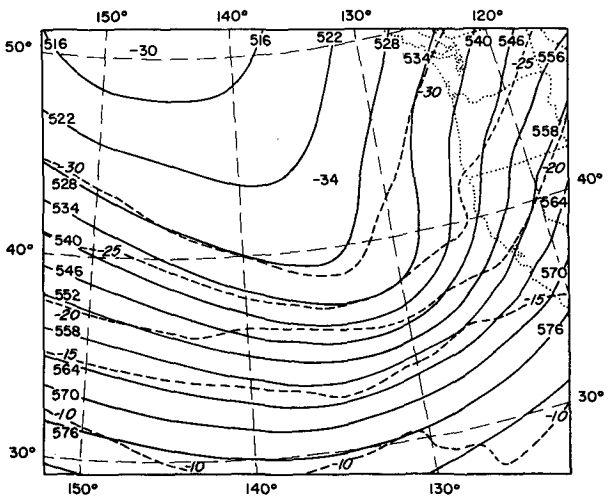

FIG. 14. The 500 mb height (dm, solid) and temperature (°C, dashed) for Experiment 4 for 24 hour forecast verifying at 0000 UTC 14 November.

17b. The maximum vorticity in the boundary layer (950 mb) at the same hour is 18.6×10^{-5} s^{-1} in the dry simulation (Fig. 17a). In the wet simulation (Fig. 17b) it is 2–3 times as large (47.7×10^{-5} s^{-1}).

The above noted differences between the dry and moist simulations are consistent with the results of many previous studies (e.g. Aubert 1957; Danard 1966; Chang et al. 1982; Chen et al. 1983; Chen and Dell'Osso 1987).

4. The impact of model physics, horizontal resolution and initial conditions

We discuss now the results of sensitivity experiments aimed at elucidating the physical processes responsible for the rapid deepening in the control experiment. Also discussed are the impacts of different parameterizations of the moisture cycle, of different grid size and of including or excluding the supplementary dataset.

a. Sensitivity to variations in model physics

Figure 18a shows the central pressure of the storm during the 24 hour period from 0000 UTC 13 November to 0000 UTC 14 November for each of the first six experiments and for the observed storm based on the analysis of RA. It should be realized that the "observed" central pressures are subject to some uncertainty, especially the pressure at 1200 UTC 13 November when few ship observations were available. These six experiments were initialized with the supplementary dataset provided by RA and were conducted with a grid resolution of 40 km. Clearly, none of the experiments succeeded in simulating the extraordinary deepening rate of 27 mb (6 h)$^{-1}$ estimated to have occurred between 1200 UTC and 1800 UTC 13 November or the

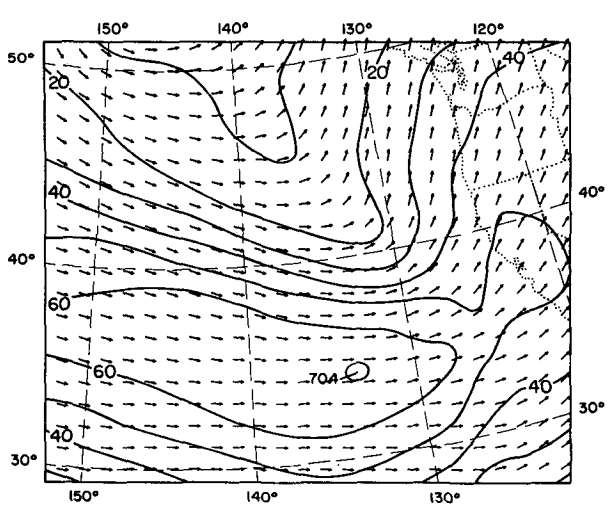

FIG. 15. The 300 mb wind field for Experiment 4 for 24 hour forecast verifying at 0000 UTC 14 November. Isotachs in m s^{-1}.

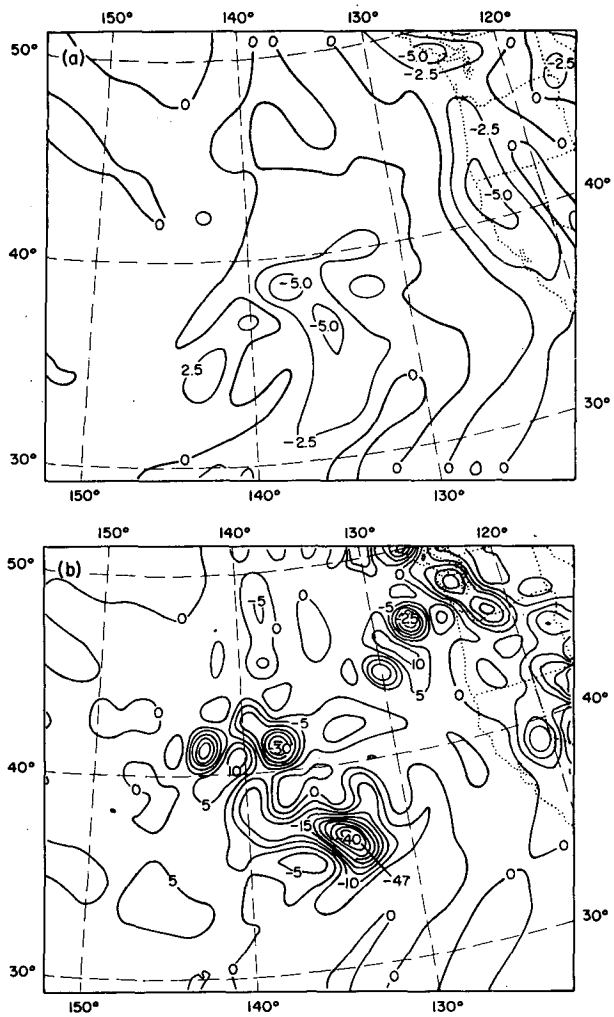

FIG. 16. The 700 mb vertical motion ($\mu b\ s^{-1}$) for (a) Experiment 4 and (b) the control experiment for 12 hour forecast verifying at 1200 UTC 13 November 1981.

full depth of the storm at 0000 UTC 14 November (950 mb). However, the three experiments incorporating latent heat release (Expts. 1–3) did produce major cyclones with central pressures in the 969–970 mb range and exhibited deepening rates [10–11 mb $(6\ h)^{-1}$ and 30–31 mb $(24\ h)^{-1}$] that qualified them as rapidly deepening storms. The dry simulations with friction (Expts. 4 and 5) resulted in deepenings of only 13–15 mb in the 24 hour period. From this we conclude that dry baroclinicity accounted for roughly half of the model deepening, the rest being attributable to moist processes and their interaction with baroclinicity.

A much smaller effect of latent heat release was found by Nuss and Anthes (1987) in a numerical investigation of rapid cyclogenesis based on synthetic data. The reason for the lesser effect in their study is not clear, but we feel that our results are in better agreement with those of other studies that have employed real data (Anthes et al. 1983; Chen et al. 1983; Chen and Dell'Osso 1987; Liou and Elsberry 1987).

The removal of friction (Expt. 6) produced an additional 5–7 mb deepening in the dry simulations. This was not sufficient however, to bring the 24 hour total to the threshold value for rapid deepening.

The 925 mb vorticity maximum (Fig. 18b) showed an even larger effect of the moist physics on the storm intensity. The dry viscid cases displayed vorticity increases from $10 \times 10^{-5}\ s^{-1}$ to about $25 \times 10^{-5}\ s^{-1}$ during the 24 hour interval. In the moist simulations the vorticity increased to 60–65 ($\times 10^{-5}\ s^{-1}$).

Removal of the surface fluxes of sensible and latent heat had little effect on storm intensity in either the moist or dry simulations. In the moist simulations (Expts. 1 and 2), the fluxes caused a slight intensification; in the dry simulations (Expts. 4 and 5) they resulted in a slightly weaker storm. This contrary behavior can be explained as follows. In the dry simu-

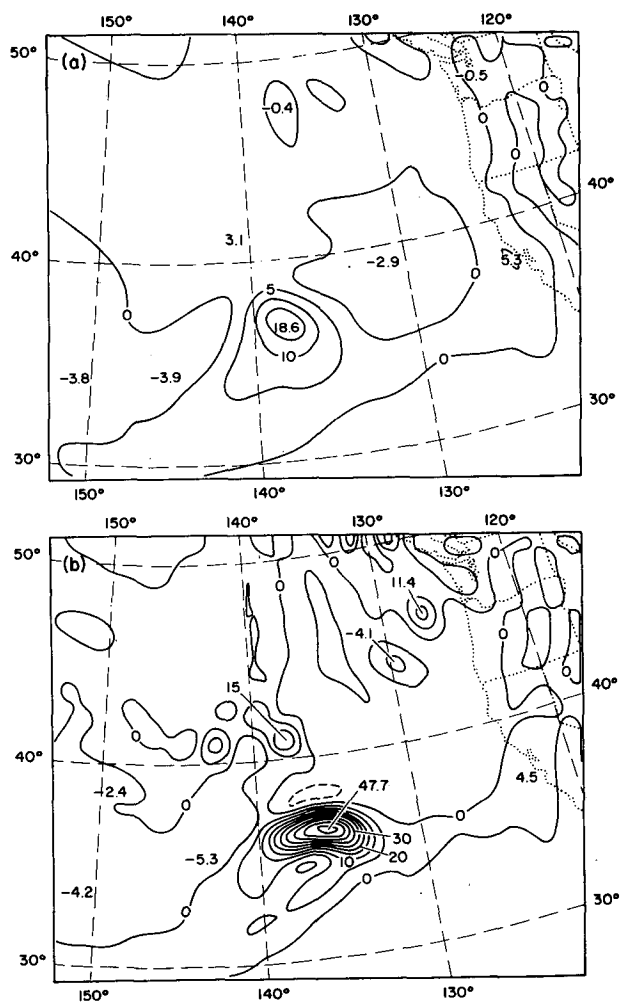

FIG. 17. The 950 mb relative vorticity ($10^{-5}\ s^{-1}$) for (a) Experiment 4 and (b) the control experiment for 12 hour forecast verifying at 1200 UTC 13 November 1981.

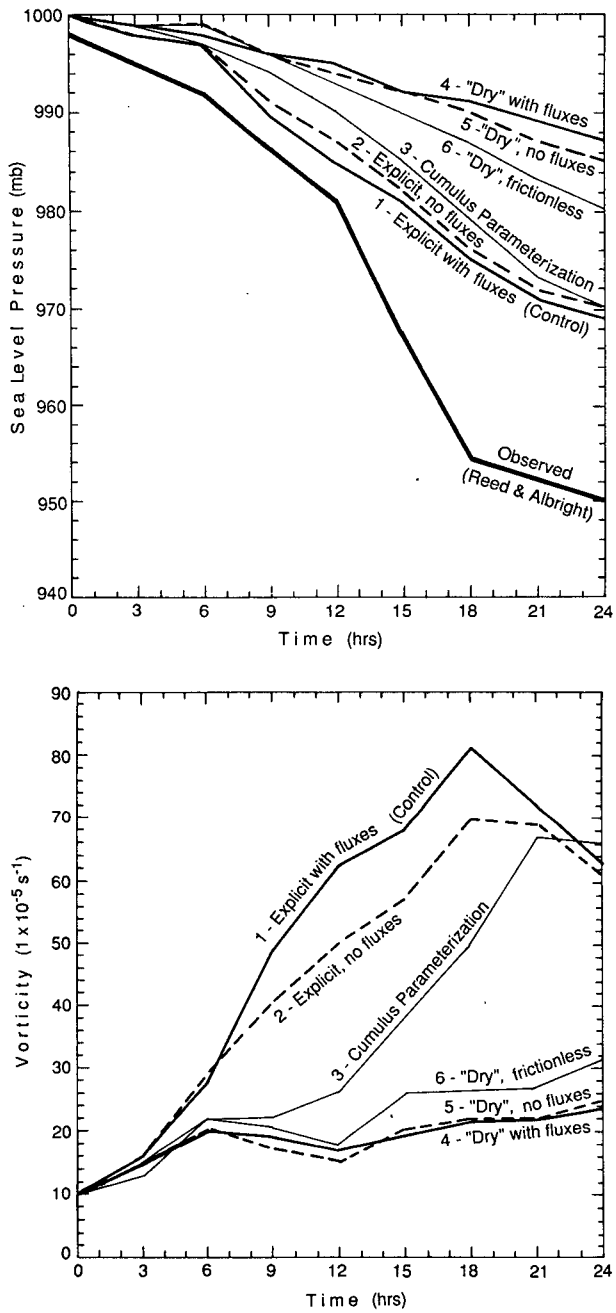

FIG. 18. (a) Central pressure, beginning at 0000 UTC 13 November, for experiments 1–6. (b) As in (a) but for the 925 mb vorticity maximum.

lations, only the sensible heat flux was allowed to heat the atmosphere. It is known from baroclinic theory (e.g., Haltiner 1971) that the pattern of sensible heating in an amplifying baroclinic wave is such as to counteract the thermal advections and thereby diminish the growth rate. In the moist simulations both sensible and latent heat fluxes were operative, and the evaporated moisture was allowed to heat the atmosphere when it condensed and precipitated. Evidently the added latent heat release was sufficient to overcome the damping effect of the sensible heating pattern.

Support for this explanation is found in Figs. 19a and 19b which compare the rainfall amounts during the final 12 hours of the moist simulations for the flux (Fig. 19a) and no flux (Fig. 19b) experiments. In the simulation with fluxes, the maximum rainfall along the storm path is 6.9 cm whereas in the no flux experiment it is 5.1 cm. The hypothesized precipitation enhancement is confirmed. The fact that the no-flux experiment produced a major cyclone with a central pressure of 970 mb indicates that the precipitable water present at the initial time was sufficient in this case to supply the precipitation and associated latent heat release needed for rapid development.

The small impact of the surface fluxes during the rapid deepening stage of the November 1981 storm is of particular interest because of the recently proposed theory of Emanuel (Emanuel 1986; Emanuel and Ro-

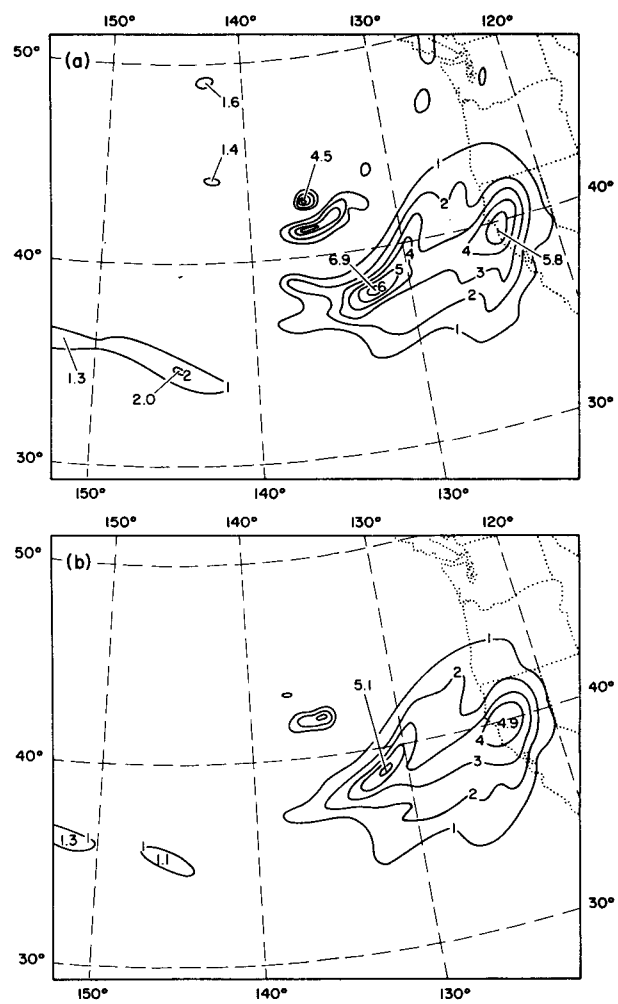

FIG. 19. Twelve hour accumulated precipitation (cm) ending at 0000 UTC 14 November for (a) control experiment and (b) Experiment 2 (without surface sensible and latent heat fluxes).

TABLE 3. Thermodynamic properties along trajectory, A_0, shown in Fig. 12.

Hour	θ (K)	θ_e (K)	T_{SST} (K)	ΔT_{sfc}[a]	Δq_{sfc}[b]	RH (%)
06	293.0	323.2	294.1	0.72	3.6	83
07	293.0	323.6	293.8	0.60	3.2	84
08	293.1	323.9	293.6	0.42	2.9	85
09	293.2	324.0	293.3	0.19	2.7	85
10	293.2	324.3	293.0	0.27	2.4	87
11	292.8	324.9	292.8	0.79	1.9	94
12	292.9	325.5	292.5	0.64	1.4	98
13	293.1	325.9	292.0	0.19	0.9	99
14	293.0	324.7	291.0	0.02	0.5	100
15	293.7	322.3	290.3	0.72	0.6	100

[a] Defined as $\Delta T_{sfc} = T_{SST} - T_{0.995}$, where $T_{0.995}$ is the temperature at the lowest model level ($\sigma = 0.995$). Unit in °C.

[b] Defined as $\Delta q_{sfc} = q_s(T_{SST}) - q_{0.995}$, where $q_{0.995}$ is the mixing ratio at the lowest model level ($\sigma = 0.995$), and $q_s(T_{SST})$ is the saturation mixing ratio based on the sea surface temperature. Unit in g kg^{-1}.

tunno 1988) for tropical storm and polar low intensification. In this theory, surface heat and moisture fluxes play a key role in the intensification by strongly raising the θ_e of the inflow air. Such a mechanism also appears attractive for explaining the small core of hurricane force winds that characterizes many explosive extratropical cyclones, including the present one. Moreover, it has been demonstrated by Uccellini et al. (1987) that, as earlier proposed by Bosart and Lin (1984), surface fluxes were essential to the development of the Presidents' Day storm.

To better document the role of surface fluxes in the present case, we present in Table 3 pertinent thermodynamic data taken along trajectory A_0 (Fig. 12), which is a representative trajectory for an inflowing air parcel. It is evident from the table that only a modest increase of θ_e occurred in the period from 0600 to 1300 UTC as the parcel approached the storm center. As the parcel traveled inward over increasingly cooler waters, the fluxes, as inferred from the temperature and mixing ratio differences, remained positive in agreement with the results of RA (their Fig. 15). But evidently the additional heat supplied by the fluxes was not enough to exert a significant effect on θ_e. Examination of 6 hourly analyses of temperature, pressure and dewpoint used in the Reed and Albright (1986) study reveal that the modeled θ_e are in good agreement with the analyzed values. We conclude that the mechanism postulated by Emanuel and Rotunno, while possibly of importance in some cases, is not an essential feature in all cases and therefore not a necessary condition for explosive deepening. The role of surface fluxes in explosive cyclogenesis will be further discussed in the concluding section.

A final noteworthy feature of Figs. 18a and 18b is the delay of approximately 9–12 hours in the time of most rapid pressure fall and vorticity rise in the experiment with parameterized convection (Expt. 3) relative to that in the control experiment. In both simulations the overall intensification was nearly the same. Insights regarding the reason for the earlier occurrence of the deepening in the control experiment are afforded by Figs. 20 and 21. These show, for both experiments, the precipitation totals during the first 12 hours of the experiments and vertical cross sections of the diabatic heating, the apparent heat source of Yanai et al. (1973), at 12 hours into the simulations (Fig. 21). The cross sections in Fig. 21 are taken along the same line as the previous cross sections (Fig. 9) for that hour (1200 UTC 13 November).

From the precipitation maps (Figs. 20a and 20b) it is evident that the maximum 12 hour accumulation in the vicinity of the storm was greater for the control experiment than for the experiment with parameterized convection. Thus, the enhanced latent heat release associated with the heavier precipitation is a possible fac-

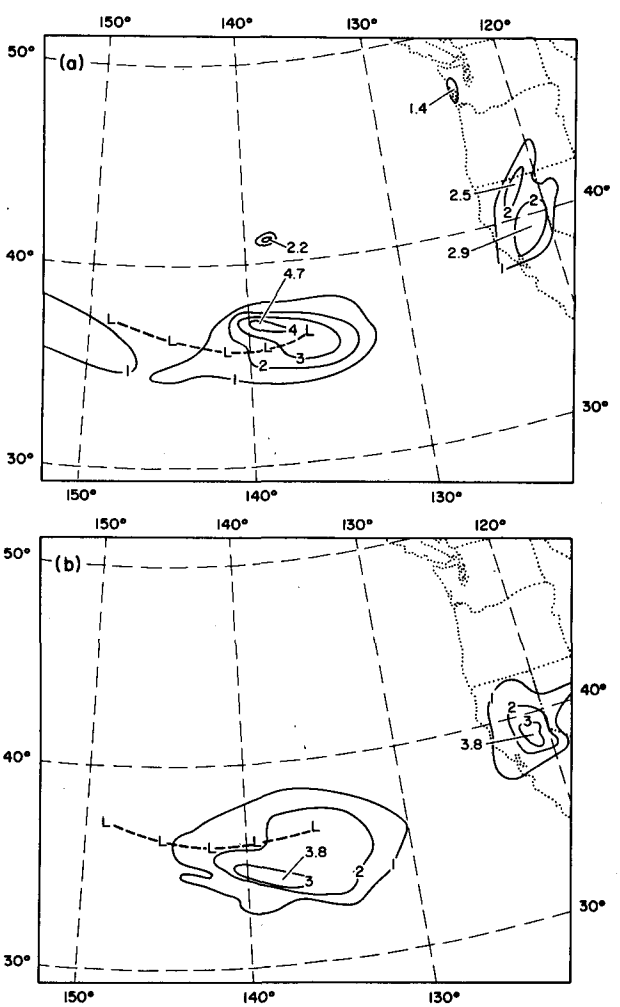

FIG. 20. Twelve hour accumulated precipitation (cm) ending at 1200 UTC 13 November for (a) control experiment and (b) Experiment 3 (with parameterized of convective and nonconvective precipitation). Dashed lines depict path of low.

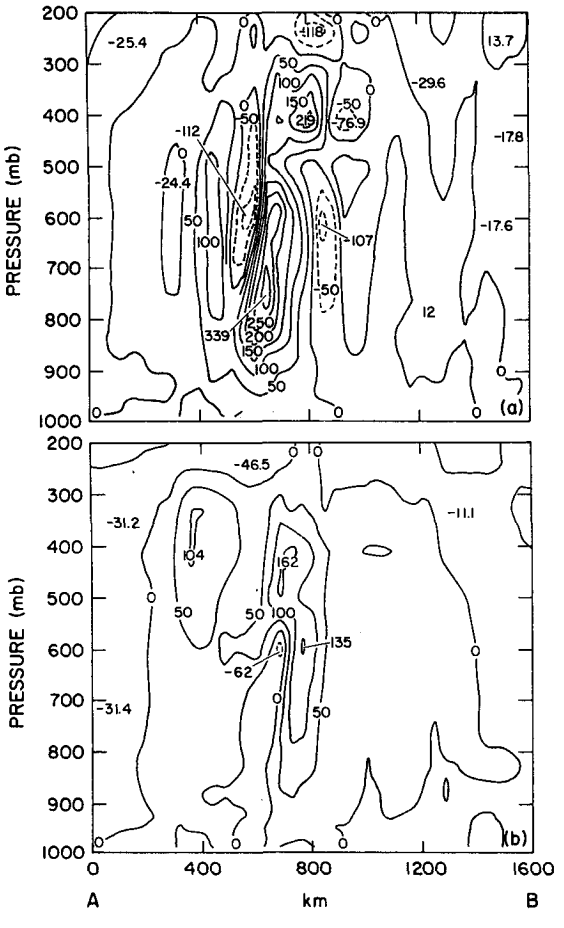

FIG. 21. Vertical cross section of apparent heat source (Q_1, in °K day^{-1}, following Kuo and Anthes 1984) at 12 hour forecast verifying at 1200 UTC 13 November for (a) control experiment and (b) Experiment 3. The position of the cross section is shown in Fig. 3a.

tor in the larger deepening rate. It is also seen from a comparison of the two maps that the maximum precipitation occurred farther to the south in Experiment 3 than in the control experiment. The more southerly location indicates that the cumulus parameterization scheme tends to displace the maximum precipitation towards the warmer, moister air.

The cross sections (Figs. 21a and 21b) show substantial differences in the heating patterns for the two experiments. Of particular significance is the difference near and just to the north of the storm center where the heating is stronger in the control experiment and the primary maximum is located at a relatively low level (750 mb). As discussed by Sardie and Warner (1985) and others, and as can be demonstrated from the quasi-geostrophic omega equation, surface development is stronger when the heating maximum is situated lower in the column. In the later stages of Experiment 3 the proportion of grid point to parameterized precipitation becomes larger and the deepening rate increases accordingly.

b. Sensitivity to horizontal resolution and initial conditions

To test the sensitivity of the simulations to horizontal resolution, an experiment (Expt. 7) was carried out that employed an 80 km grid rather than the previous 40 km grid, but that was in every other way identical to the control experiment (Expt. 1). Comparison of the results of the two experiments reveals little impact of grid size on the central pressure of the storm (Fig. 22a), which suggests that the failure of the control experiment to achieve a sufficiently deep storm would

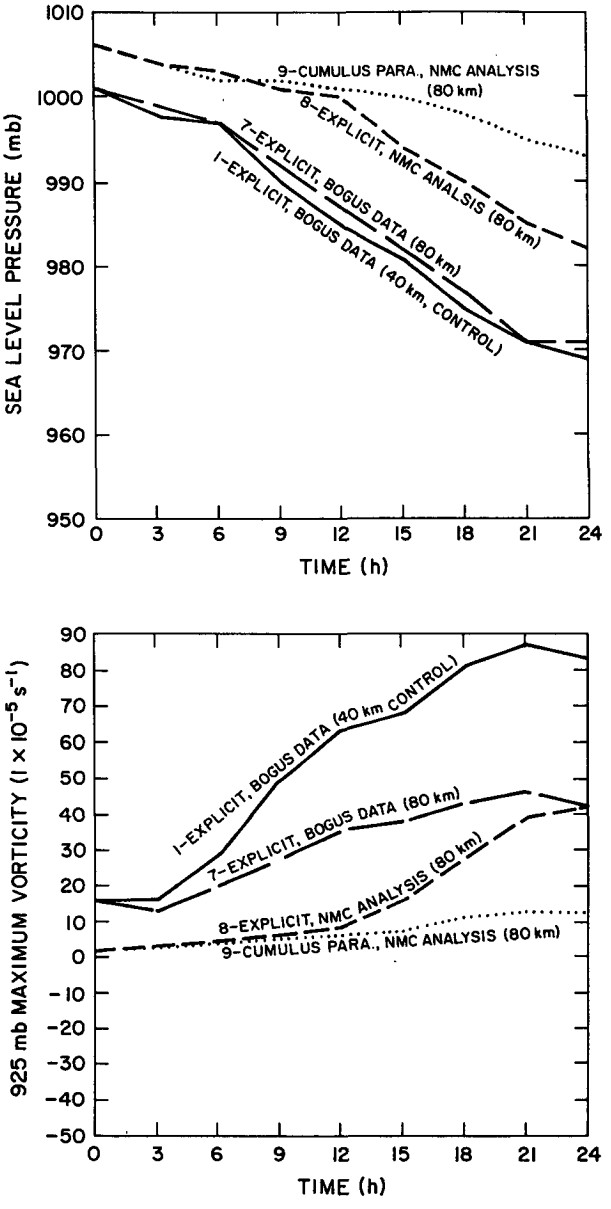

FIG. 22. (a) Central pressure and (b) the 925 mb vorticity maximum, beginning at 0000 UTC 13 November, for experiments 7–9 and the control experiment.

not be overcome simply by increasing the horizontal resolution. This conclusion does not mean that a fine grid is not required in order to properly simulate the storm. Obviously, an even finer grid than the 40 km grid is needed in order to resolve adequately the inner core shown in Fig. 4b.

The grid size did, however, have a substantial impact on the 925 mb vorticity (Fig. 22b). The final intensity of the vorticity maximum was roughly twice as great in the higher resolution control experiment (Expt. 1) than in Experiment 7. Clearly, the explicit convection scheme that was used in both of these experiments produces more intense vorticity features as the grid size is reduced. The differences in the sensitivity of central pressure and 925 mb maximum vorticity to horizontal resolution is a consequence of the inherently different scales of pressure and vorticity variations (Hoskins et al. 1985).

The sensitivity of the simulations to initial conditions can be seen by comparing the results of Experiment 7 to those of Experiment 8, an experiment in which the supplementary data were withheld but which was otherwise identical to Experiment 7. Deficiencies of the NMC analysis used in Experiment 8 were documented in RA. They include a surface low that lacks sufficient depth and an insufficiently warm and moist boundary layer in the warm sector of the low. Another view of the deficient strength of the low is afforded by Fig. 23 which contrasts the initial 925 mb vorticity field of the NMC analysis (Fig. 23a) with that used in Experiment 7 (Fig. 23b). The latter analysis, which is strongly influenced by the delayed ship reports, shows a vorticity maximum that is an order of magnitude larger than that portrayed in the NMC analysis.

Without the supplementary data, the start of the deepening of the storm was delayed (Fig. 22a) and the final central pressure was not as low (982 mb vs 971 mb). The starting pressure was higher by about 5 mb. In the case of the 925 mb vorticity (Fig. 22b) a similar retardation occurred, but the final vorticity was the same in both experiments. The results of these experiments indicate that the supplementary data had two main impacts: they caused the rapid deepening to commence earlier, in agreement with observations, and they produced a deeper storm.

As mentioned in the Introduction, the LFM forecast failed completely to predict the storm development. In contrast, a storm of moderate depth formed in Experiment 8, which, like the LFM run, lacked the supplementary data. In order to ascertain the cause(s) of the discrepancy, an additional experiment (Expt. 9) was conducted on the 80 km grid with the supplementary data withheld but with parameterized rather than explicit convection. Both the LFM and the PSU/NCAR mesoscale model used variations of the Kuo scheme in the convective parameterization. Comparison of the results of Experiments 8 and 9 indicates

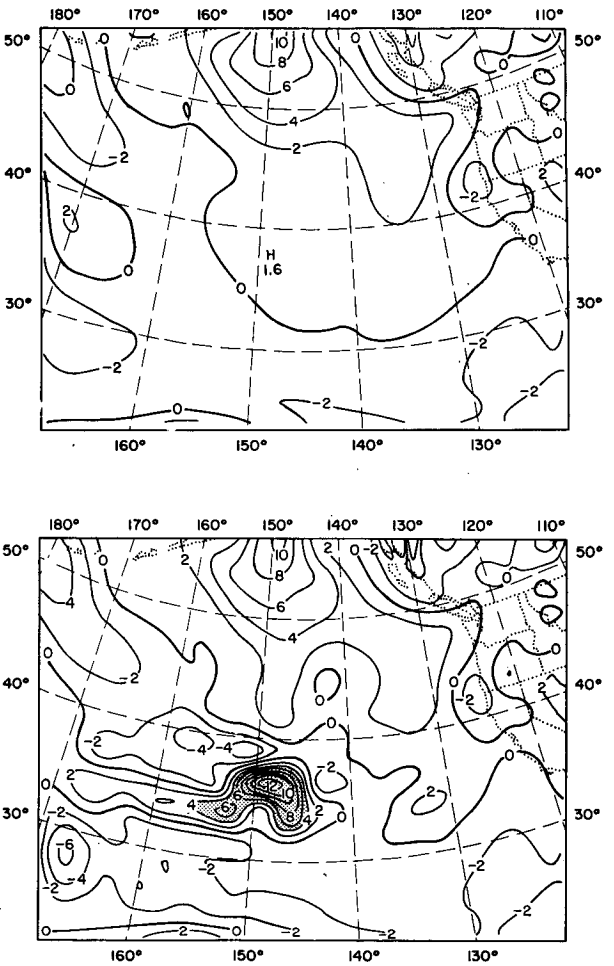

FIG. 23. The 925 mb relative vorticity (10^{-5} s^{-1}) at 0000 UTC 13 November for (a) the NMC analysis and (b) the enhanced analysis based on the supplementary dataset of Reed and Albright (1986).

(Fig. 22a) a much lesser deepening in the simulation with parameterized convection (993 mb vs 982 mb) and an even longer delay than before in the onset of the deepening. Why the LFM forecast failed to deepen at all is still not certain. Likely causes are the coarser grid employed by the LFM and, particularly, differences between the LFM initial fields (no longer retrievable in digital form) and the fields from the NMC final analysis. The latter fields form the basis of the present simulations.

Finally, it should be noted that it would be incorrect to conclude from the results of Experiments 8 and 9 that use of the explicit scheme generally leads to excessive deepening. In the previously described experiments utilizing the supplementary data and the 40 km grid (Expts. 1 and 3) the final pressure was essentially the same for the explicit and parameterized schemes. Corresponding simulations with an 80 km grid (not shown) gave a similar result.

5. Summary and discussion

A remarkable explosive cyclogenesis that occurred in the eastern Pacific on 13 November 1981 has been documented by Reed and Albright (1986). A deepening rate of approximately 40 mb in 12 hours was observed at one stage in the development. At the peak of the storm the central pressure attained a depth of 950 mb or below. Winds of well-above hurricane force were reported from two ships caught in the storm. The LFM operational model initialized at 0000 UTC on 13 November completely failed to predict the development.

In this paper we present the results of numerical experiments aimed at 1) testing the ability of the latest version of the PSU/NCAR mesoscale model to simulate the storm development, 2) elucidating the role of various physical processes in the development and 3) understanding the cause of the failure of the NMC operational forecasts. Six 24 hour experiments, initialized at 0000 UTC 13 November, were carried out on a 40 km grid with use of the NMC operational analysis for that hour supplemented by a special dataset prepared by Reed and Albright. The object of these experiments was to examine the sensitivity of the simulations to various physical factors, including latent heat release, surface energy fluxes, surface friction and the parameterization of convection. Three additional experiments were carried out on an 80 km grid to determine 1) the impact of horizontal resolution, 2) the impact of the supplementary dataset, and 3) the performance of the model when run in a mode most closely resembling that of the LFM model.

A control experiment that employed the 40 km grid, the supplementary dataset and a full representation of physical processes (but without parameterized convection) best reproduced the actual storm. It formed a major low with central pressure of 969 mb, and exhibited a deepening rate of 31 mb in the 24 hour period. This rate exceeds that required for explosive deepening. However, the values for the central pressure and deepening rate fell considerably short of the observed. The motion of the storm was well predicted, as the simulated position after 24 hours and 1800 km of travel differed from the observed position by only 150 km.

Other verifiable features that were reproduced well were 1) cloud and moisture patterns observed in satellite images, including a striking dark area with low values of middle and upper tropospheric humidity seen in the water vapor channel at the time of the most rapid deepening, and 2) a sharp, narrow upper-level trough that was missing from the NMC analysis but the existence of which was well supported by aircraft winds. Because of the presence of this upper-level feature, which was located immediately to the rear of the surface low, the 1000–500 mb thickness field did not possess the warm central core at 0000 UTC 14 November shown in the analysis of RA (Fig. 4b). It is possible that the warm core was a fictitious feature that resulted from subtracting correctly analyzed 1000 mb heights from incorrectly analyzed 500 mb heights in a region where midtropospheric data were sparse or absent.

The upper-level trough is shown to be a product of the moist physics, because this feature did not appear in the dry simulations. It is also shown that the dry simulations produced a weaker storm development in terms of the depth of the central pressure, the thermal gradient near and ahead of the storm center and the magnitudes of the vertical motion and vorticity.

The vertical structure of the simulated storm was examined by taking cross sections through the system at 1200 UTC 13 November and 0000 UTC 14 November. Features of special interest shown by the sections are: 1) a leaning forward with height of the simulated cold front, or leading edge of the cold advection, even prior to the occluded stage, 2) extremely large wind gradients and vorticities in the lower troposphere and 3) large values of potential vorticity in the lower troposphere. The large potential vorticity appeared mainly in cloudy air, suggesting that it was created by condensation heating. Large values of potential vorticity were also found in stratospheric air that descended to 700–500 mb and approached the storm from the rear. The stratospheric air tended to circle the storm center rather than to become collocated with it.

For the purpose of examining the role of symmetric instability in the development, an additional cross section containing fields of equivalent potential temperature, absolute momentum and vertical velocity was constructed for 1200 UTC 13 November. This section revealed that a symmetrically neutral, or even slightly unstable, condition prevailed near the storm center at that hour. A narrow, sloping region of strong ascent, marked by upward velocities in excess of 50 cm s^{-1} in the middle and lower troposphere, was present near the warm boundary of the zone of weak stability or instability. Such strong upward motions occurring in proximity to the surface represent a potent source of low-level vorticity, as was verified from hourly measurements of divergence and vorticity taken along three trajectories that entered the interior of the storm. Between 0600 and 1200 UTC vorticities along the trajectories increased from near zero to 6–8 f with most of the increase taking place in the last few hours of travel. Horizontal convergences in excess of 1×10^{-4} s^{-1} were simulated during the period of rapid spinup.

From these results we conclude that symmetric instability (or neutrality) may be an important factor in rapid cyclogenesis. Its role can be understood, at least in part, from the Sawyer–Eliassen equation (Sawyer 1956; Eliassen 1962), which is commonly used to measure the transverse ageostrophic circulation that forms in response to frontogenetical forcing. In this

equation, based on the geostrophic momentum or semigeostrophic system of equations, the potential vorticity plays the same role in determining the response of the vertical motion to the baroclinic forcing that the static stability does in the quasi-geostrophic system. Given the same forcing, the smaller the potential vorticity, the larger the vertical motion. The relevance of the potential vorticity in the present context is that within the framework of the Sawyer–Eliassen equation, it measures the degree of symmetric stability (Hoskins 1974). When symmetric stability prevails, it is positive. Under neutral conditions it is zero, and when the atmosphere is symmetrically unstable, it is negative. The effect of weak or neutral stability (small or zero potential vorticity) in enhancing frontal circulations has been well demonstrated by Emanuel (1985) and Thorpe and Emanuel (1985).

Although the Sawyer–Eliassen equation yields valuable insights regarding the role of symmetric instability, it is not fully suitable for the purpose. First, the equation is only solvable for the stable case when the ellipticity condition is satisfied and, second, it presupposes two-dimensional flow. An even larger response to the forcing can be visualized when moist or moist conditional instability exists. However, the effect cannot be determined from the equation since it becomes hyperbolic in the unstable case. Also, the criterion for symmetric instability of negative potential vorticity is based on the assumption of straight, two-dimensional flow. It is not clear that this is the correct criterion in curved, three-dimensional flow. These issues require further study.

Whatever the outcome of these issues, it is apparent from the work of Hoskins and Draghici (1977) with the semigeostrophic equations that, in three dimensions as in two, it is the potential vorticity that determines the strength of the vertical motions that form in response to a given forcing, and hence the intensity of the development. We may, therefore, identify the potential vorticity as the basic factor in the rapid development and leave in abeyance the question of its relationship to symmetric instability in the three-dimensional case.

Principal findings of the sensitivity experiments are:

1) Latent heat release had a major impact on the storm development. All moist simulations produced explosive deepening. None of the dry simulations attained the required 24 mb $(24\ h)^{-1}$ mark, including a simulation conducted without surface friction. On the basis of the relative deepenings of the dry and moist simulations, it is concluded that about half the deepening in the control run could be attributed to dry baroclinicity and half to moist processes and their interaction with baroclinicity. This finding is consistent with the results of other studies that have compared wet and dry simulations in real cases.

2) Withdrawal of the surface fluxes of sensible and latent heat had only a minor impact. The fluxes had a small damping effect in the dry experiments and a slight amplifying effect in the moist experiments. From these results it is inferred that sensible heat flux inhibited the storm development and latent heat flux enhanced it, but only when the added water vapor was allowed to enter the precipitation cycle. Although the fluxes were of little consequence during the period of rapid development, they were undoubtedly important in creating the favorable initial state, as documented in RA.

Our finding that the concurrent fluxes had only a slight effect (3 percent enhancement) on the rapid deepening is only one of a wide range of findings on the issue. Nuss and Anthes (1987) found that the fluxes reduced the deepening by 29 percent in their idealized case and Danard and Ellenton (1980) found a 10 percent reduction in a real case off the east coast of North America. On the other hand, moderate to large enhancements have been reported in some cases: 25 percent in the *QE-II* storm by Anthes et al. (1983) and 127 percent by Uccellini et al. (1987) along the Carolina coast immediately prior to the explosive stage of the Presidents' Day storm. It is possible that the enhancement was much less at the time of most rapid deepening.

The widely varying influence of the surface fluxes can be understood in terms of the quasi-geostrophic ω-equation and geographical factors. According to the ω-equation, a positive diabatic heating anomaly contributes to cyclonic development. Such an anomaly occurs in regions of positive surface flux of sensible heat and in regions where latent heat is released by condensation and precipitation. Surface latent heat flux does not enter directly into the equation. In a typical oceanic storm that conforms to the Norwegian cyclone model and/or is well removed from coastal influences, the pattern of surface heating (Petterssen et al. 1962) is not conducive to development, since the maximum heating occurs far to the rear of the cyclone, not in and ahead of it. The negative effect can, however, be counteracted by surface moisture fluxes to the degree that the fluxes add moisture, *as the storm is in progress* that increases the frontal precipitation in and ahead of it. If the atmosphere is already sufficiently moistened by *antecedent* fluxes, the effect of the *concurrent* fluxes will be small. On the other hand, near the east coasts of continents, where the air mass modification is rapid, the effect of the concurrent fluxes can be large. Moreover, the sensible heat fluxes can also exert a positive effect through coastal frontogenesis and secondary cyclogenesis induced by the juxtaposition of air heated from below by the warm ocean currents and cold, unmodified continental air trapped near the shore (Uccellini et al. 1987).

An inescapable conclusion of the foregoing discussion is that the mechanism of rapid deepening is not

tied directly to surface fluxes. In some cases concurrent fluxes are required for the mechanism to operate; in other cases they are not.

3) The 24 hour simulations with and without convective parameterization produced equally intense storms, but the rapid deepening took place considerably sooner in the simulation with explicit or grid resolvable precipitation than in the simulation with parameterization of subgrid scale precipitation. Further diagnosis revealed that during the first 12 hours of the simulations the experiment with the explicit scheme produced heavier precipitation, and therefore greater condensation heating than the experiment with parameterized convection. Perhaps more significantly, the further diagnosis also revealed that the maximum diabatic heating at hour 12 (1200 UTC 13 November) occurred lower in the atmosphere in the experiment without parameterization than in the experiment with it. This situation also favored more rapid deepening at earlier stages.

4) Reduction of the grid size from 80 to 40 km, with the model physics and initial conditions left unchanged, had little effect on the central pressure of the storm. From this, we conclude that it is unlikely that a further reduction in grid size would in itself eliminate the substantial difference between the observed and simulated depths.

5) The experiment run without the supplementary dataset revealed that poorer definition of the initial state had two impacts: first, it delayed the onset of the deepening; second, it produced a weaker storm. The experiment with identical physics and horizontal resolution but with the supplementary data included yielded a storm that was more than 10 mb deeper.

6) The experiment designed to match most closely the conditions under which the LFM operational forecast was carried out (80 km grid, Kuo-type cumulus parameterization, NMC analysis with no supplementary data) gave by far the weakest development of the nine simulations. The reason why this experiment produced a weak storm when the LFM failed to produce even a slight depression is not certain. One possible reason is that, because of the difference in data cutoff times, the NMC final or operational analysis used in the present simulations better defined the initial state than did the earlier analysis used by the LFM.

The question still remains why the experiments failed to capture the full extremity of the development. In this respect we note that current operational models, such as the ECMWF T106 model, the U.K. Meteorological Office regional model and the NMC Nested Grid Model (NGM), employ physics similar to the PSU/NCAR model and have comparable horizontal and vertical resolutions. Occasionally these models have great success in predicting explosive cyclogenesis. Thus, model physics, grid size and lateral boundary conditions may not be the crucial elements in the failure to simulate the observed depth of the November 1981 storm. We cannot overlook the fact that despite the addition of supplementary data, which unquestionably led to a more accurate depiction of low-level features, considerable uncertainties exist regarding the initial analyses at middle and upper levels. Sharp features can exist at these levels that are crucial to rapid development, as shown by Bosart (1981) and Uccellini et al. (1985) for the Presidents' Day storm. From inspection of a series of 6 hourly ECMWF 500 and 250 mb charts, that display analyzed vorticity and isotach fields, respectively, and contain plotted upper air soundings and aircraft and satellite winds, we believe that the upper level trough that formed in conjunction with the storm cannot be directly associated with a preexisting short-wave trough or jet streak of unusual intensity that entered the region from far upstream, i.e., from an arc extending from Alaska to Japan. However, the ECMWF charts reveal sharper vorticity features in the neighborhood of the incipient low (and in general) than do the NMC analyses that formed the basis of our initialization. It is quite possible that sharper features existed aloft than shown in the NMC analyses—and indeed even in the ECMWF analyses.

In this respect, it should be commented that, through the courtesy of ECMWF, a special simulation of the storm was run commencing from 0000 UTC 13 November 1981, with the version of the T106 system in operation in 1986 and with reassimilation of the archived data. Since the ECMWF forecasts are made only once daily at 1200 UTC, no operational forecasts were available from 0000 UTC 13 November. The special forecast for 0000 UTC 14 November yielded a surface low with central pressure of 985 mb displaced about 350 km northeast of the true position. This forecast, which did not have the advantage of the bogus data, started with a surface low or trough that was intermediate in intensity between that depicted on the NMC operational analysis (Fig. 16a of RA) and that shown in the manual analysis (Fig. 3d of RA). It is not known how much of the deepening of the T106 simulated storm in excess of the 993 mb figure obtained in Experiment 9 is attributable to the sharper low-level features and how much to the sharper features aloft. In any event, we cannot rule out the possibility that a substantial part of the forecast error in our control simulation may have stemmed from deficiencies in the upper-level analyses.

The final answer to the problem of explosive oceanic cyclogenesis must await the acquisition of datasets that fully sample all relevant aspects of the marine environment and further development of numerical models that better represent the physical processes associated with latent heat release and the marine boundary layer.

Acknowledgments. We thank Richard Anthes for initiating this project, Mark Albright, Warren Blier,

Clifford Mass, Richard Rotunno and Da-Lin Zhang for fruitful discussions, Jian-Wen Bao, Evelyn Donall, David Gill, and Prasad Govindarajan for programming assistance, and Joyce Case for editorial support. We also thank two anonymous reviewers and Lance F. Bosart, Randall M. Dole, Frederick Sanders and Louis W. Uccellini for helpful comments. One of us, R.J.R., is deeply grateful to A. Hollingsworth, W. A. Heckley and A. J. Simmons for supplying the ECMWF analyses and forecasts while he was on sabbatical leave at the European Centre. The research of one of the authors (R.J.R.) was supported by the National Science Foundation under Grant ATM-8421396-01. The model runs were performed on a Cray X-MP/4800 computer, through a grant from the Pittsburgh Supercomputing Center. The diagnostic calculations were performed on the NCAR Cray X-MP/4800 and the Mesoscale and Microscale Meteorology Division VAX-8530.

REFERENCES

Anthes, R. A., 1977: A cumulus parameterization scheme utilizing a one-dimensional cloud model. *Mon. Wea. Rev.*, **105**, 270–286.

——, Y.-H. Kuo and J. R. Gyakum, 1983: Numerical simulations of a case of explosive cyclogenesis. *Mon. Wea. Rev.*, **111**, 1174–1188.

——, E.-Y. Hsie and Y.-H. Kuo, 1987: *Description of the Penn State/NCAR Mesoscale Model Version 4 (MM4)*. NCAR Tech. Note, NCAR/TN-282+STR, 66 pp. [National Center for Atmospheric Research, P.O. Box 3000, Boulder, CO 80307.]

Aubert, E. J., 1957: On the release of latent heat as a factor in large-scale atmospheric motions. *J. Meteor.*, **14**, 527–542.

Benjamin, S. G., and N. L. Seaman, 1985: A simple scheme for objective analysis in curved flow. *Mon. Wea. Rev.*, **113**, 1184–1198.

Bennetts, D. A., and B. J. Hoskins, 1979: Conditional symmetric instability—a possible explanation for frontal rainbands. *Quart. J. Roy. Meteor. Soc.*, **105**, 945–962.

Blackadar, A. K., 1979: High resolution models of the planetary boundary layer. *Advances in Environmental Science and Engineering*, 1, No. 1, Pfafflin and Zeigler, Eds., Gordon and Breach, 50–85.

Bosart, L. F., 1981: The Presidents' Day snowstorm of 18–19 February 1979: A subsynoptic-scale event. *Mon. Wea. Rev.*, **109**, 1542–1566.

——, and S. C. Lin, 1984: A diagnostic analysis of the Presidents' Day storm of February 1979. *Mon. Wea. Rev.*, **112**, 2148–2177.

Boyle, J. S., and L. F. Bosart, 1986: Cyclone–anticyclone couplets over North America. Part II: Analysis of a major cyclone event over the Eastern United States. *Mon. Wea. Rev.*, **114**, 2432–2465.

Brown, R. A., 1986: On satellite scatterometer capabilities in air–sea interaction. *J. Geophys. Res.*, **91**(C2), 2221–2232.

Chang, C. B., D. J. Perkey and C. W. Kreitzberg, 1982: A numerical case study of the effects of latent heating on a developing wave cyclone. *J. Atmos. Sci.*, **39**, 1555–1570.

Chen, S.-J., and L. Dell'Osso, 1987: A numerical case study of East Asian coastal cyclogenesis. *Mon. Wea. Rev.*, **115**, 477–487.

Chen, T.-C., C.-B. Chang and D. J. Perkey, 1983: Numerical study of an AMTEX '75 oceanic cyclone. *Mon. Wea. Rev.*, **111**, 1818–1829.

Danard, M. B., 1966: Further studies with a quasi-geostrophic model incorporating effects of released latent heat. *J. Appl. Meteor.*, **5**, 388–395.

——, and G. E. Ellenton, 1980: Physical influences on East Coast cyclogenesis. *Atmos.-Ocean*, **18**, 65–82.

Delsol, F., K. Miyakoda and R. H. Clarke, 1971: Parameterized processes in the surface boundary layer of an atmospheric circulation model. *Quart. J. Roy. Meteor. Soc.*, **97**, 181–208.

Eliassen, A., 1962: On the vertical circulation of frontal zones. *Geofys. Publ.*, **24**(4), 147–160.

Emanuel, K., 1983: On assessing local conditional symmetric instability from atmospheric soundings. *Mon. Wea. Rev.*, **111**, 2016–2033.

——, 1985: Frontal circulations in the presence of small moist symmetric stability. *J. Atmos. Sci.*, **42**, 1062–1071.

——, 1986: An air–sea interaction theory for tropical cyclones. Part I: Steady state maintenance. *J. Atmos. Sci.*, **43**, 585–604.

——, and R. Rotunno, 1988: Polar lows as Arctic hurricanes. *Tellus*, in press.

——, M. Fantini and A. J. Thorpe, 1987: Baroclinic instability in an environment of small stability to slantwise moist convection. Part I: Two-dimensional models. *J. Atmos. Sci.*, **44**, 1559–1573.

Errico, R. M., 1986: *Initialization of NCAR/PSU Mesoscale Model.* NCAR Tech. Note, NCAR/TN-270+1A, 120 pp. [NCAR, P.O. Box 3000, Boulder, CO 80307.]

Gyakum, J. R., 1983a: On the evolution of the *QE II* storm. I: Synoptic aspects. *Mon. Wea. Rev.*, **111**, 1137–1155.

——, 1983b: On the evolution of the *QE II* storm. II. Dynamic and thermodynamic structure. *Mon. Wea. Rev.*, **111**, 1156–1173.

Haltiner, G. J., 1971: *Numerical Weather Prediction*, First ed. Wiley and Sons, 317 pp.

Holton, J. R., 1979: *An Introduction to Dynamic Meteorology.* Academic Press, 391 pp.

Hoskins, B. J., 1974: The role of potential vorticity in symmetric stability and instability. *Quart. J. Roy. Meteor. Soc.*, **100**, 480–482.

——, and I. Draghici, 1977: The forcing of ageostrophic motion according to the semigeostrophic equations and in an isentropic coordinate model. *J. Atmos. Sci.*, **34**, 1859–1867.

——, M. E. McIntyre and A. W. Robertson, 1985: On the use and significance of isentropic potential vorticity maps. *Quart. J. Roy. Meteor. Soc.*, **111**, 877–946.

Hsie, E.-Y., R. A. Anthes and D. Keyser, 1984: Numerical simulation of frontogenesis in a moist atmosphere. *J. Atmos. Sci.*, **41**, 2581–2594.

Kuo, H. L., 1974: Further studies of the parameterization of the influence of cumulus convection on large scale flow. *J. Atmos. Sci.*, **31**, 1232–1240.

Kuo, Y.-H., and R. A. Anthes, 1984: Mesoscale budgets of heat and moisture in a convective system over the central United States. *Mon. Wea. Rev.*, **112**, 1482–1497.

Leary, C., 1971: Systematic errors in operational National Meteorological Center primitive equation surface prognoses. *Mon. Wea. Rev.*, **99**, 409–413.

Liou, C.-S., and R. L. Elsberry, 1987: Heat budgets of analyses and forecasts of an explosively deepening maritime cyclone. *Mon. Wea. Rev.*, **115**, 1809–1824.

Nuss, W. A., and R. A. Anthes, 1987: A numerical investigation of low-level processes in rapid cyclogenesis. *Mon. Wea. Rev.*, **115**, 2728–2743.

Petterssen, S., D. L. Bradbury and K. Pederson, 1962: The Norwegian cyclone models in relation to heat and cold sources. *Geofys. Publ.*, **24**, 243–280.

Reed, R. J., and M. D. Albright, 1986: A case study of explosive cyclogenesis in the eastern Pacific. *Mon. Wea. Rev.*, **114**, 2297–2319.

Roebber, P. J., 1984: Statistical analysis and updated climatology of explosive cyclones. *Mon. Wea. Rev.*, **112**, 1577–1589.

Rosenthal, S. L., 1978: Numerical simulation of tropical cyclone development with latent heat release by the resolvable scales I: Model description and preliminary results. *J. Atmos. Sci.*, **35**, 258–271.

Ross, B. B., and I. Orlanski, 1982: The evolution of an observed cold front. Part I: Numerical simulation. *J. Atmos. Sci.*, **39**, 296–327.

Sanders, F., 1987: Skill of NMC operational dynamic models in pre-

diction of explosive cyclogenesis. *Wea. and Forecasting,* **2,** 322–336.

——, and J. R. Gyakum, 1980: Synoptic-dynamic climatology of the "bomb." *Mon. Wea. Rev.,* **108,** 1589–1606.

Sardie, J. M., and T. T. Warner, 1985: A numerical study of the development mechanisms of polar lows. *Tellus,* **37A,** 460–477.

Sawyer, J. S., 1956: The vertical circulation at meteorological fronts and its relation to frontogenesis. *Proc. Roy. Soc. London,* **A234,** 246–262.

Thorpe, A. J., and K. Emanuel, 1985: Frontogenesis in the presence of small stability to slantwise convection. *J. Atmos. Sci.,* **42,** 1809–1824.

Uccellini, L. W., 1986: The possible influence of upstream upper-level baroclinic processes on the development of the *QEII* storm. *Mon. Wea. Rev.,* **114,** 1019–1027.

——, P. J. Kocin, R. A. Petersen, C. H. Wash and K. F. Brill, 1984: The Presidents' Day cyclone of 18–19 February 1979: Synoptic overview and analysis of the subtropical jet streak influencing the pre-cyclogenetic period. *Mon. Wea. Rev.,* **112,** 31–55.

——, D. Keyser, K. F. Brill and C. H. Wash, 1985: Presidents' Day cyclone of 18–19 February 1979: Influence of upstream trough amplification and associated tropopause folding on rapid cyclogenesis. *Mon. Wea. Rev.,* **113,** 962–988.

——, R. A. Petersen, K. F. Brill, P. J. Kocin and J. J. Tuccillo, 1987: Synergistic interactions between an upper level jet streak and diabatic processes that influence the development of a low level jet and a secondary coastal cyclone. *Mon. Wea. Rev.,* **115,** 2227–2261.

Wang, B., and I. Orlanski, 1987: Study of a heavy rain vortex formed over the eastern flank of the Tibetan plateau. *Mon. Wea. Rev.,* **115,** 1370–1393.

Yanai, M., S. Esbensen and J. Chu, 1973: Determination of bulk properties of tropical cloud clusters from large-scale heat and moisture budgets. *J. Atmos. Sci.,* **30,** 611–627.

Zhang, D.-L., and R. A. Anthes, 1982: A high-resolution model of the planetary boundary layer-sensitivity tests and comparisons with SESAME-79 data. *J. Appl. Meteor.,* **21,** 1594–1609.